AN ABSTRACT OF THE THESIS OF

DENNIS WILLIAM FRITZ (Name) for the MASTER OF SCIENCE (Degree)

in MECHANICAL ENGINEERING (Major) presented on May 12, 1967 (Date)

Title: THE PHOTOELASTIC COATING METHOD APPLIED TO THE STRESS ANALYSIS OF WOOD

Redacted for Privacy

Abstract approved: Dr. Hans Dahlke

The merits of the photoelastic coating technique as applied to wood were evaluated. Comparative tests were made on 12 nominal two-by-four Douglas Fir boards. The object of these tests was to determine the limitations of this technique, such as accuracy and complexity of experimental procedure. Correlation of the experimental results was achieved by determining the modulus of elasticity for each board from load-deflection measurements, (1) at midpoint loading, (2) at third-point loading, (3) from strain gage readings, and (4) from photoelastic coating data. A linear regression analysis was used to find 90% and 95% confidence intervals of accuracy for the photoelastic data.

As an application, the coating technique was used to investigate the stress distribution around butt joints in six-ply laminated beams.

The Photoelastic Coating Method Applied to the Stress Analysis of Wood

by

Dennis William Fritz

A THESIS

submitted to

Oregon State University

in partial fulfillment of
the requirements for the
degree of

Master of Science

June 1967

APPROVED:

Redacted for Privacy

Associate Professor of Mechanical Engineering
in charge of major

Redacted for Privacy

Head of Department of Mechanical and Industrial Engineering

Redacted for Privacy

Dean of Graduate School

Date thesis is presented May 12, 1967

Typed by Eula Weathers and Gwen Hansen for Dennis William Fritz

ACKNOWLEDGMENT

The author wishes to express his sincere gratitude to all those who assisted in this project. Unfortunately, space does not allow each individual to be cited, but certain persons should be singled out.

First and foremost, I am indebted to my Major Professor, Hans J. Dahlke, who went far above the call of duty in the direction and fulfillment of this project.

Second, I wish to thank the other graduate students for their physical assistance and moral support.

Third, my heartfelt thanks go to Jack Kellogg for his assistance and the use of his facilities in the construction of the apparatus used in the experimental work.

Financially I am indebted to the Weyerhaeuser Company and the Engineering Experiment Station for their support in the project.

Finally, I must cite Type-Ink and their typists for their patience and assistance in the completion of this thesis.

TABLE OF CONTENTS

LIST OF FIGURES

LIST OF TABLES

THE PHOTOELASTIC COATING METHOD APPLIED TO THE STRESS ANALYSIS OF WOOD

I. INTRODUCTION

The Need for Experimental Stress Analysis in the Wood Industry

The challenge to wood as a structural material has greatly increased in the past few years. Other materials have become more competitive because advances in their technologies have made them more economical. To meet the challenge for more efficient and better utilization of wood products, a more exact wood technology is required. Two areas in this technology have been particularly static but have considerable promise for improving the economics of the lumber industry. These are the areas of structural design and stress grading.

Structural design with wood requires the stress analysis of structural members and joints as well as the determination of stress concentration factors caused by holes, notches, and mechanical fasteners. Wood is a complex material, and the simplified theory applied to homogeneous, isotropic materials such as steel does not accurately describe the stress distribution in wood structures. To avoid the complexities of a more accurate theory, designers and engineers have applied this simplified theory to wood and have

compensated for its inadequacies with conservative safety factors. An effective experimental stress analysis technique could help reduce these safety factors by adding to the basic understanding of joints and stress concentrations, and by leading to the development of simple and accurate empirical equations. Such equations would reduce the waste caused by overdesign and would increase the economy of using wood as a structural material.

Another area of conservative safety factors and resultant waste is stress grading. This is the rating of sawn lumber according to its expected working stress capabilities. Presently, most stress grading is done by experienced men who simply inspect the lumber as it comes from the mill and mark each piece according to the number of noticeable strength reducing factors such as knots, checks, splits, and grain slope. This method is an estimation of strength rather than a measurement. Conservative estimates are necessary to assure that each piece is not overrated. High speed non-destructive testing methods are now being employed in some lumber mills to eliminate the guesswork in stress grading, and the most common of these mechanically measures the stiffness of each board assuming a direct correlation between stiffness and strength. However, none of the new methods for automatic stress grading can accurately predict the effects of the strength reducing factors. An effective stress analysis technique could be used to find relationships between

various irregularities in wood and the stress concentrations caused by them. More accurate stress grading would be possible because of these relationships and more economical lumber utilization would result.

An effective technique would have numerous additional applications in the field of wood technology. The areas of wood plasticity, wood creep, wood laminates, and combined loading of wooden structural members all require a supplemental accurate stress analysis method.

Scope of the Thesis

The present investigation is the product of a research grant made by the Weyerhaeuser Company to the Engineering Experiment Station, Oregon State University and is designed to evaluate the photoelastic coating technique as it applies to wood. To do this, comparative tests were made on nominal two-by-four Douglas Fir boards. The object of these tests was to determine the limitations of this technique, such as accuracy and complexity of experimental procedure. For the tests, 12 beams were loaded both at the center and third points on a 39 inch span. To correlate the experimental results, the modulus of elasticity for each board was determined from load-deflection measurements, strain gage readings, and photoelastic coating data. In addition the strain distributions

predicted by strain gages were compared with those predicted by the photoelastic coating.

A problem of particular concern to the Weyerhaeuser Company was then chosen as an application of the coating technique. For lumber produced by laminating veneer, it is important to know the effects of the joints in the veneer on the strength of the laminated member. For lumber constructed of butt joined, quarter inch Douglas Fir veneer laminae, the following questions were investigated.

1. At what distance must butt joints be separated to eliminate the interaction of their individual stress concentrations?

2. To what extent does the size of the gap at a butt joint affect the stress concentration caused by the joint?

3. To what extent does a well glued butt joint reduce the stress concentration caused by the joint?

4. Is there a significant difference between the stress concentrations caused by butt joints in compression and butt joints in tension?

5. What is the approximate magnitude of the stress concentration caused by a butt joint?

In addition to the presentation of these results, this thesis includes a literature review in the field of experimental stress analysis applied to wood (particularly photoelasticity). The review

embodies a brief history of experimental stress analysis in wood research with a bibliography. It is restricted to material given in the Forestry Abstracts since 1945, the Proceedings of the Society for Experimental Stress Analysis, various symposia on photo-elasticity and non-destructive testing, and texts on elasticity, experimental stress analysis, and wood technology.

II. PREVIOUS APPLICATIONS OF EXPERIMENTAL STRESS ANALYSIS TO WOOD

Stresses are determined experimentally by strain measurements. There are two categories classifying these measurements: point-by-point and whole-field methods. Any experimental technique measuring strain over a very small area is considered a point-by-point method. Examples of this type are extensometers or mechanical strain gages and electric resistance strain gages. A method measuring the varying strains over a much larger area is considered a whole-field method. Examples are brittle coatings, Moiré grids, and photoelastic coatings.

Because of the complex nature of wood, experimental stress analysis techniques have not been widely used. Some researchers have reported successful applications, however, and many of these are cited in the following sections.

Point-By-Point Methods

Extensometers

There are many types of instruments which mechanically, optically, or electrically measure the change in length between two knife edges bearing on a strained surface. These are generally classified as extensometers and have been used by many researchers

in the wood industry. Most have the capabilities for accurate measurement of small strains but usually require a large gage length over which the strain is averaged. This requirement has restricted their use mainly to uniform stress field problems such as determining the mechanical properties of various wood species, and finding the stress in loaded structural members.

Electric Resistance Strain Gages

Electrical resistance strain gages have been applied to general stress analysis problems in wood with greater success. For many years the U. S. Forest Products Laboratory has used strain gages for various investigations. Their experience is presented in a report by Youngquist (51). Other researchers have also developed techniques and studied limitations of strain gages applied to wood (1, 36, 49). Radcliffe (34) developed a method for determining the nine elastic constants of wood using strain gages.

One of the principal advantages of the strain gage is its ability to measure the average strain over a very small area. Thus, investigators are nearly able to measure strain at a point although this is not necessarily an advantage with wood. Wood is a very inhomogeneous material partly because of the annual variations in growth, i.e., spring and summerwood. Even in the simplest case of a uniform uniaxial state of stress, strains from point to point across

the growth rings will vary greatly. Consequently, the experimenter must be careful to cover a representative whole number of annual rings with his strain gage in order to obtain a representative value. This is often difficult since common strain gages available are seldom an integral number of annual rings in length. The principal disadvantage of the strain gage (and all point-by-point methods) is that only a single point on the surface can be investigated at one time. A problem of finding the maximum strain location on a large surface would require the mounting of many strain gages in a trial and error manner until this location was found.

Whole-Field Methods

Brittle Coatings

This method employs a brittle lacquer which is applied to the test surface. When loaded, the strains on the surface cause cracks in the lacquer which appear perpendicular to the principal tensile strain. The number of cracks per unit length indicates the magnitude of this strain.

A few investigators have applied this method to wood. Procedures and techniques have been outlined by Maku and Sasaki (25, 26) and by Yavorski and Cunningham (5). The latter researchers also applied the method to analysis of strain in a glue block shear test

specimen (50). Others have used the method to find the stress directions around a wood cutter (22) and to determine the mechanical properties of wood (16).

Difficulties arise because the lacquer does not crack in compression and compressive strains must be determined by a complicated procedure. In most cases a complete quantitative stress analysis is laborious and subject to considerable error. Also, the techniques for correct application of the lacquer to wood are exacting and difficult especially with respect to the high moisture sensitivity of the brittle coating. Brittle coating is most useful with qualitative problems involving tensile strains.

Moiré Grids

In this method a grid of equally spaced lines is fixed to the test specimen before it is loaded. As the specimen is strained the fixed grid is distorted. This distortion is made visible by placing a master grid of the same spacing as the original undeformed grid over the distorted grid. Interference fringes appear and the inclination and spacing of these fringes supply the surface strain data. To obtain complete strain data the interference fringe pattern must be observed for two separate master grid orientations.

A disadvantage with the Moiré method is that accurate strain analysis in the elastic range of most materials requires extremely

fine and therefore expensive grids.

To the writer's knowledge, Moiré techniques have not been applied to the stress analysis of wood.

Photoelastic Coatings

To use this method, a special transparent plastic coating is cemented to the test surface so that it takes on the strains of the surface when the structure is loaded. The properties of the plastic create optical interference patterns when the plastic is illuminated with polarized light and these patterns are related to the principal strains and the principal strain directions.

This technique has been applied to complex stress analysis of wood with greater success than any of the previous methods. Morris and Jansson (28) made one of the first such applications by studying the stress distribution in the neighborhood of a knot. Schniewind (35) used the method to investigate the mechanism of check formation in the drying of wood. Takahashi and Nakato (42, 43, 44) made more extensive studies. Initially they investigated the properties of epoxies as they related to various ratios of the component resins. The properties included photoelastic sensitivity, strain sensitivity, creep, temperature sensitivity, and modulus of elasticity. Their purpose was to find suitable coatings for wood research. Next, they used the brittle lacquer technique to show that strains on the surface

of wood are not always equivalent to strains measured by the plastic coating. Finally, they used the method to study the strains on the face of a log in diametral compression. Stieda (40, 41) has probably presented the most complete and useful report on the photoelastic coating method applied to wood. In addition to presenting the basic theory of wood elasticity and the techniques of coatings, he made three applications of interest. He studied the stress distributions near a concentrated load, along the rim of a hole in a compression member, and along a circular notch in the tension side of a beam in pure bending.

In spite of the work done by Stieda and others, the photoelastic coating method applied to wood is still in early stages. Studies of accuracy, limitations, and improved techniques are needed.

III. ORTHOTROPIC ELASTICITY

Orthotropic Theory Related to Wood

The theory of orthotropic elasticity deals with stress-strain relations in homogeneous elastic solids having three perpendicular planes of elastic symmetry. Examples of such solids are cold rolled metals because of property changes in the direction of rolling and some individual crystals because of their orthogonal atomic make-up. Wood is approximately an orthotropic material because of its three perpendicular natural directions, i.e., longitudinal (L) with the grain, tangential (T) to growth rings, and radial (R) to the growth rings. The orthogonal axes as they apply to wood are shown in Figure 1. The elastic properties in each of these directions is different, often radically, from those properties in the other directions. Wood is not exactly rectangularly orthotropic, however, because of the curvature of the growth rings. The theory applies best to wood in which this curvature is small, i.e., lumber cut from near the bark, and becomes less accurate toward the center of the tree. Cylindrical coordinates might overcome this deficiency but would lead to laborious computations when applied to the usual problems with square sawn lumber. Wood is also not strictly homogeneous. The alternate layers of spring and summerwood account for some of this and natural imperfections such as knots for the rest. Thus,

wood is only an approximate orthotropic solid and limitations of the orthotropic elastic theory as applied to wood must be recognized. In spite of the limitations a number of investigators (17, 27, 29, 30, 38, 49) have made successful applications.

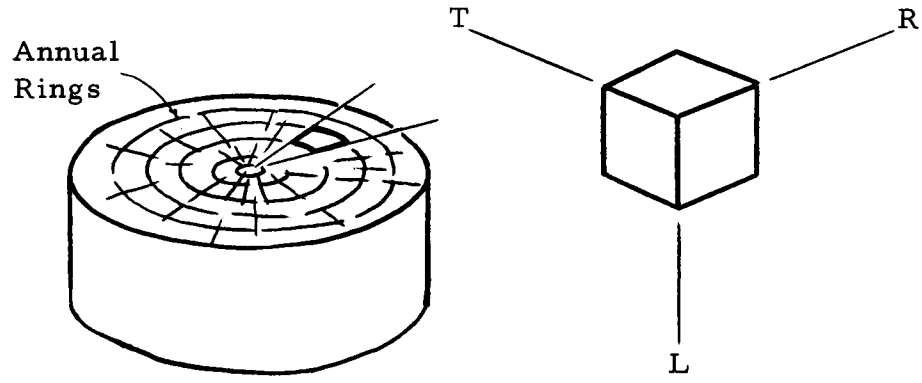

Figure 1. Orthotropic axes in wood.

Some useful portions of the theory are presented in the following sections. A complete treatment of the subject is given in the references (17, 18, 19, 23, 27, 29, 30, 38, 40).

Hooke's Law

The most general form of Hooke's Law giving strains in terms of stresses can be written:

$$
\begin{aligned}
\epsilon_{xx} &= S_{11}\tau_{xx} + S_{21}\tau_{yy} + S_{31}\tau_{zz} + S_{41}\tau_{yz} + S_{51}\tau_{zx} + S_{61}\tau_{xy} \\
\epsilon_{yy} &= S_{12}\tau_{xx} + S_{22}\tau_{yy} + S_{32}\tau_{zz} + S_{42}\tau_{yz} + S_{52}\tau_{zx} + S_{62}\tau_{xy} \\
\epsilon_{zz} &= S_{13}\tau_{xx} + S_{23}\tau_{yy} + S_{33}\tau_{zz} + S_{43}\tau_{yz} + S_{53}\tau_{zx} + S_{63}\tau_{xy} \\
\epsilon_{yz} &= S_{14}\tau_{xx} + S_{24}\tau_{yy} + S_{34}\tau_{zz} + S_{44}\tau_{yz} + S_{54}\tau_{zx} + S_{64}\tau_{xy} \\
\epsilon_{zx} &= S_{15}\tau_{xx} + S_{25}\tau_{yy} + S_{35}\tau_{zz} + S_{45}\tau_{yz} + S_{55}\tau_{zx} + S_{65}\tau_{xy} \\
\epsilon_{xy} &= S_{16}\tau_{xx} + S_{26}\tau_{yy} + S_{36}\tau_{zz} + S_{46}\tau_{yz} + S_{56}\tau_{zx} + S_{66}\tau_{xy}
\end{aligned}
\tag{1}
$$

where x, y, z represent the standard rectangular coordinates.

τ_{yz} is the stress component on the y face of an element acting in the z direction.

ϵ_{yz} is the strain component on the y face of an element acting in the z direction.

S_{ij} are the stiffness coefficients embodying the elastic constants of the material.

Sokolnikoff (39, p. 63) points out that for an orthotropic material, the most general form of Hooke's Law has nine independent elastic constants and can be written:

$$
\begin{aligned}
\epsilon_{xx} &= S_{11}\tau_{xx} + S_{21}\tau_{yy} + S_{31}\tau_{zz} \\
\epsilon_{yy} &= S_{12}\tau_{xx} + S_{22}\tau_{yy} + S_{23}\tau_{zz} \\
\epsilon_{zz} &= S_{13}\tau_{xx} + S_{23}\tau_{yy} + S_{33}\tau_{zz} \\
\epsilon_{yz} &= S_{44}\tau_{yz} \\
\epsilon_{zx} &= S_{55}\tau_{zx} \\
\epsilon_{xy} &= S_{66}\tau_{xy}
\end{aligned}
\tag{2}
$$

where the x, y, and z axes are coincident with the axes of elastic symmetry in the material. The number of independent stiffnesses above are reduced to nine by the relations,

$$S_{ij} = S_{ji} \qquad (i, j = 1, 2, 3, 4, 5, 6) \tag{3}$$

Elastic Constants

The stiffness coefficients can be identified in terms of the common elastic constants by examination of Eqs. (2).

S_{11} must be the normal strain ϵ_{xx} per unit normal stress τ_{xx}.

S_{21} must be the normal strain ϵ_{xx} per unit normal stress τ_{yy}.

S_{66} must be the shear strain ϵ_{xy} per unit shear stress τ_{xy}.

S_{22}, S_{33}, S_{31}, S_{12}, S_{23}, S_{13}, S_{23}, S_{44}, and S_{55} are similarly defined.

Eqs. (4) can be deduced from the above statements.

$$\begin{aligned} S_{11} &= 1/E_x & S_{44} &= 1/G_{yz} \\ S_{22} &= 1/E_y & S_{55} &= 1/G_{zx} \\ S_{33} &= 1/E_z & S_{66} &= 1/G_{xy} \\ \\ S_{21} &= \nu_{yx}/E_y & S_{12} &= \nu_{xy}/E_x \\ S_{31} &= \nu_{zx}/E_z & S_{13} &= \nu_{xz}/E_x \\ S_{23} &= \nu_{yz}/E_y & S_{32} &= \nu_{zy}/E_z \end{aligned} \tag{4}$$

Further, since $S_{ij} = S_{ji}$,

$$\begin{aligned} \nu_{yx}/E_y &= \nu_{xy}/E_x \\ \nu_{zx}/E_z &= \nu_{xz}/E_x \\ \nu_{yz}/E_y &= \nu_{zy}/E_z \end{aligned} \tag{5}$$

where in Eqs. (4) and (5),

E_x is the modulus of elasticity in the x direction.

G_{xy} is the modulus of rigidity or shear modulus relating to shear in the xy plane.

ν_{xy} is the Possion's ratio of contraction (extension) in the y direction to unit imposed extension (contraction) in the x direction.

Axis Rotation

Hearmon (18, p. 26) has listed the general formulae derived by Voigt (48) which determine the new stiffness coefficients due to a coordinate rotation. For a rotation θ about the z-axis as shown in Figure 2, the stiffnesses corresponding to the new primed axes are given by Eqs. (6).

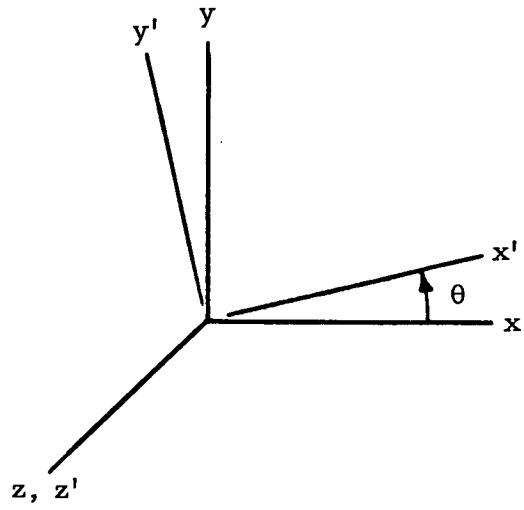

Figure 2. Axis rotation.

$$
\begin{aligned}
S'_{11} &= S_{11}m^4 + (2S_{21} + S_{66})n^2m^2 + S_{22}n^4 && = 1/E'_x \\
S'_{22} &= S_{11}n^4 + (2S_{21} + S_{66})n^2m^2 + S_{22}m^4 && = 1/E'_y \\
S'_{33} &= S_{33} && = 1/E'_z \\
S'_{44} &= S_{44}m^2 + S_{55}h^2 && = 1/G'_{yz} \\
S'_{55} &= S_{44}n^2 + S_{55}m^2 && = 1/G'_{zx} \\
S'_{66} &= 4(S_{11} + S_{22} - 2S_{21})m^2n^2 + S_{66}(m^2 - n^2)^2 && = 1/G'_{xy} \\
S'_{21} &= (S_{11} + S_{22})m^2n^2 + S_{21}(m^4 + n^4) - S_{66}m^2n^2 && = -\nu'_{yx}/E'_y \quad (6) \\
S'_{31} &= S_{32}n^2 + S_{31}m^2 && = -\nu'_{zx}/E'_z \\
S'_{32} &= S_{32}m^2 + S_{31}n^2 && = -\nu'_{zy}/E'_z \\
S'_{54} &= (S_{44} - S_{55})mn \\
S'_{61} &= -2(S_{11}m^2 - S_{22}n^2)mn + (2S_{21} + S_{66})mn(m^2 - n^2) \\
S'_{62} &= -2(S_{11}n^2 - S_{22}m^2)mn - (2S_{21} + S_{66})mn(m^2 - n^2) \\
S'_{63} &= 2(S_{32} - S_{31})mn
\end{aligned}
$$

where $n = \sin\theta$ $\quad m = \cos\theta$

Note that the last four stiffnesses are newly introduced by the rotation. There are still only nine independent constants, however, since these new ones are expressible in terms of the original nine stiffnesses.

Elastic Constants in Wood

If Eqs. (4) are substituted into the first nine of Eqs. (6), equations relating the elastic constants of different coordinate systems are derived. Further, if the x y z system is replaced by the T R L system, then the Eqs. (7) will result.

$$\frac{1}{E'_T} = \frac{m^4}{E_T} + \left(\frac{1}{G_{TR}} - \frac{2\nu_{RT}}{E_R}\right) m^2 n^2 + \frac{n^4}{E_R}$$

$$\frac{1}{E'_R} = \frac{n^4}{E_T} + \left(\frac{1}{G_{TR}} - \frac{2\nu_{RT}}{E_R}\right) m^2 n^2 + \frac{m^4}{E_R}$$

$$E'_L = E_L$$

$$\frac{1}{G'_{LT}} = \frac{m^2}{G_{RL}} + \frac{n^2}{G_{LT}}$$

$$\frac{1}{G'_{LT}} = \frac{n^2}{G_{RL}} + \frac{m^2}{G_{LT}}$$

$$\frac{1}{G'_{TR}} = 4\left(\frac{1}{E_T} + \frac{1}{E_R} + \frac{2\nu_{RT}}{E_R}\right) m^2 n^2 + \frac{1}{G_{TR}} (m^2 - n^2)^2$$

$$\frac{\nu'_{RT}}{E'_R} = \frac{\nu'_{TR}}{E'_T} = \left(\frac{1}{G_{TR}} - \frac{1}{E_T} - \frac{1}{E_R}\right) m^2 n^2 + (m^4 + n^4) \frac{\nu_{RT}}{E_R}$$

$$\frac{\nu'_{LT}}{E'_L} = \frac{\nu'_{TL}}{E'_T} = \frac{\nu_{LR}}{E_L} n^2 + \frac{\nu_{LT}}{E_L} m^2 \qquad (7)$$

$$\frac{\nu'_{LR}}{E'_L} = \frac{\nu'_{RL}}{E'_R} = \frac{\nu_{LR}}{E_L} m^2 + \frac{\nu_{LT}}{E_L} n^2$$

where again, $n = \sin\theta$ and $m = \cos\theta$.

Eqs. (7) apply to the situation shown in Figure 3 and are particularly useful because most sawn lumber has its faces cut parallel with the elastic longitudinal axis, i.e., parallel with the grain, but seldom parallel with the growth rings.

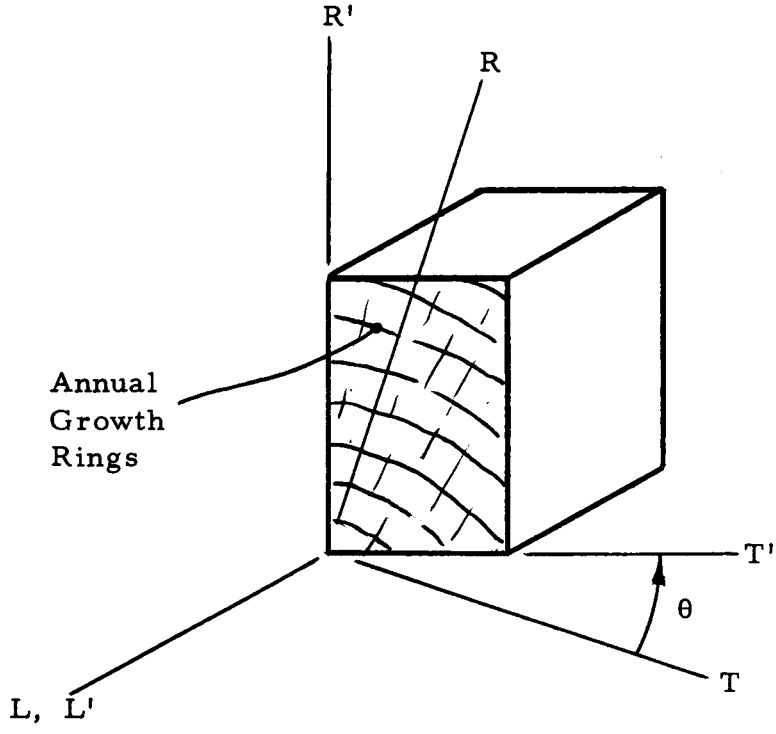

Figure 3. Rotation of axes in wood.

Stress and Strain Directions

The most serious difficulty with the stress analysis of an orthotropic material is that the directions of principal stress do not in general coincide with the directions of principal strain as they always do in isotropic solids. They do coincide only when the principal stresses lie along axes of elastic symmetry. An example of this non-coincidence is seen by examining Hooke's Law as it applies to the rotated set of coordinates in Figure 2. This form of Hooke's Law with the stiffness coefficients given by Eqs. (6) appears as Eqs. (8).

$$
\begin{aligned}
\epsilon'_{xx} &= S'_{11}\tau'_{xx} + S'_{21}\tau'_{yy} + S'_{31}\tau'_{zz} + S'_{61}\tau'_{xy} \\
\epsilon'_{yy} &= S'_{12}\tau'_{xx} + S'_{22}\tau'_{yy} + S'_{32}\tau'_{zz} + S'_{62}\tau'_{xy} \\
\epsilon'_{zz} &= S'_{13}\tau'_{xx} + S'_{23}\tau'_{yy} + S'_{33}\tau'_{zz} + S'_{63}\tau'_{xy} \\
\epsilon'_{yz} &= S'_{44}\tau'_{yz} + S'_{54}\tau'_{zx} \\
\epsilon'_{zx} &= S'_{45}\tau'_{yz} + S'_{55}\tau'_{zx} \\
\epsilon'_{xy} &= S'_{16}\tau'_{xx} + S'_{26}\tau'_{yy} + S'_{36}\tau'_{zz} + S'_{66}\tau'_{xy}
\end{aligned}
\tag{8}
$$

Now consider a case of uniaxial tension not coincident with an axis of elastic symmetry as shown in Figure 4 for which Eqs. (8) apply.

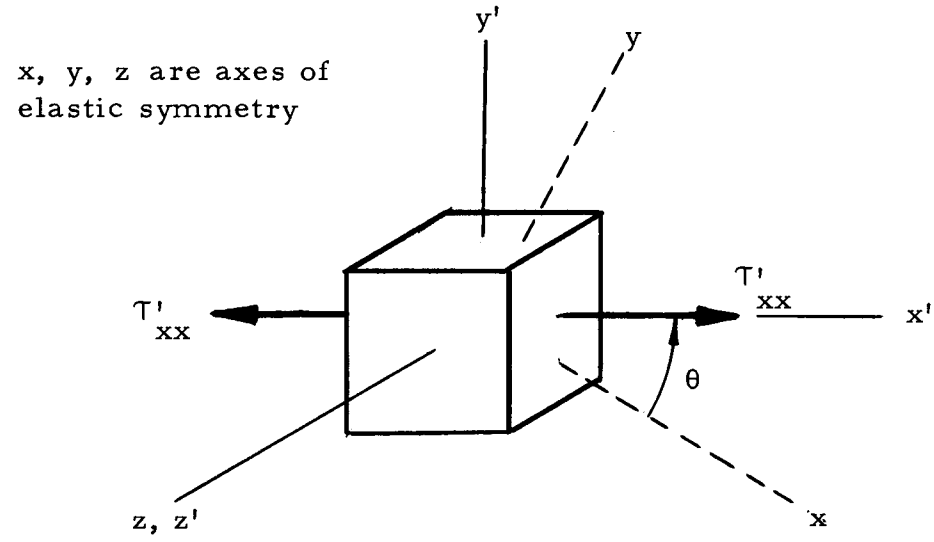

Figure 4. Tension element.

Disregarding the strain in the z direction, Eqs. (8) reduce to Eqs. (9).

$$\begin{aligned} \epsilon'_{xx} &= S'_{11}\tau'_{xx} \\ \epsilon'_{yy} &= S'_{12}\tau'_{xx} \\ \epsilon'_{xy} &= S'_{16}\tau'_{xx} \end{aligned} \tag{9}$$

This state of stress can be represented on a Mohr's circle as shown in Figure 5.

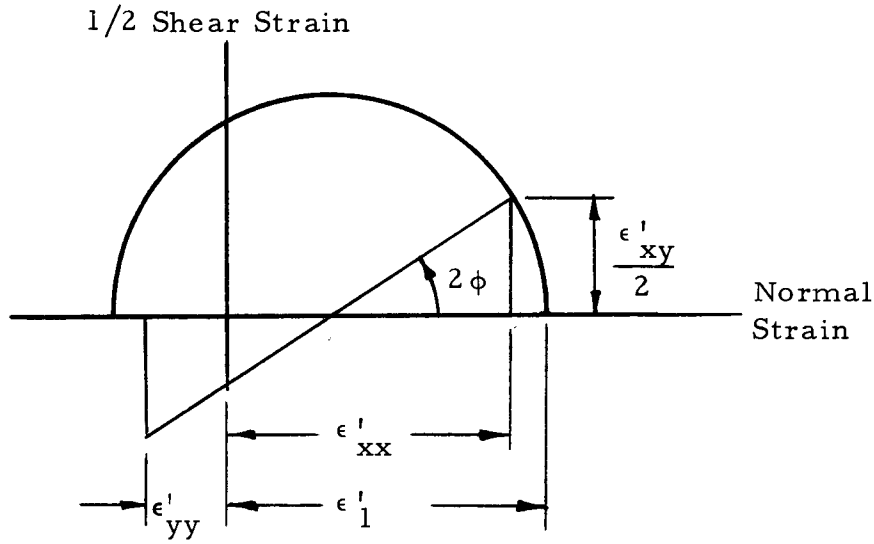

Figure 5. Mohr's circle for strain.

where ϵ'_1 is the magnitude of the maximum principal strain

and ϕ is the angle between the direction of the principal strain and the direction of normal strain (the latter direction is also that of the principal stress τ_{xx}).

Clearly, since ϕ is non-zero the directions of principal stress and strain do not coincide. Because of this noncoincidence, strain directions and magnitudes experimentally measured on the surface cannot usually be related easily to stresses but must be converted by the complex orthotropic elastic theory.

IV. PHOTOELASTICITY AND THE PHOTOELASTIC COATING METHOD

The theory of photoelasticity is based on the physical fact that most transparent solids (some more than others) have indices of refraction that change in proportion to the magnitudes and directions of the principal strains that exist in the solid. These property changes can be observed optically and related directly to strain and hence through the theory of elasticity to stress. The basic principles of photoelasticity have been known since the early 19th century, but not until the early 20th century were they applied by Coker and Filon (4) to engineering problems. Much important work with the method has been done since. References (8, 10, 13, 15, 20, 21) give a complete account of the present photoelastic technology. Some fundamentals of the theory are presented in the following sections.

Experimental Stress Analysis Requirements

The complete determination of the surface stress at a point implies two sufficient conditions.

1. The directions of the principal stresses at that point must be known.
2. The magnitudes of these principal stresses must be known.

There are many ways for an investigator to find these conditions experimentally but all rely on measuring surface strains and

theoretically relating them to stresses. The photoelastic coating technique provides the necessary surface strain data by measurement of optical patterns.

Polarized Light

Consider light as electromagnetic vibrations similar to radio waves with the different colors characterized by different wavelengths or frequencies. White light is composed of an entire spectrum of wavelengths and monochromatic light is composed of a single wavelength. Ordinary white light originating, for example, from the sun or an incandescent source, has electromagnetic vibrations in all directions; Figure 6 shows such a source. If this kind of light passes through a polarizing filter, it becomes polarized and has its vibrations confined to a single plane parallel with the polarizing axis. The polarizing filter absorbs all other vibrations. Clearly, a second polarizing film with its axis at right angles to the first will cause extinction, as shown in Figure 6.

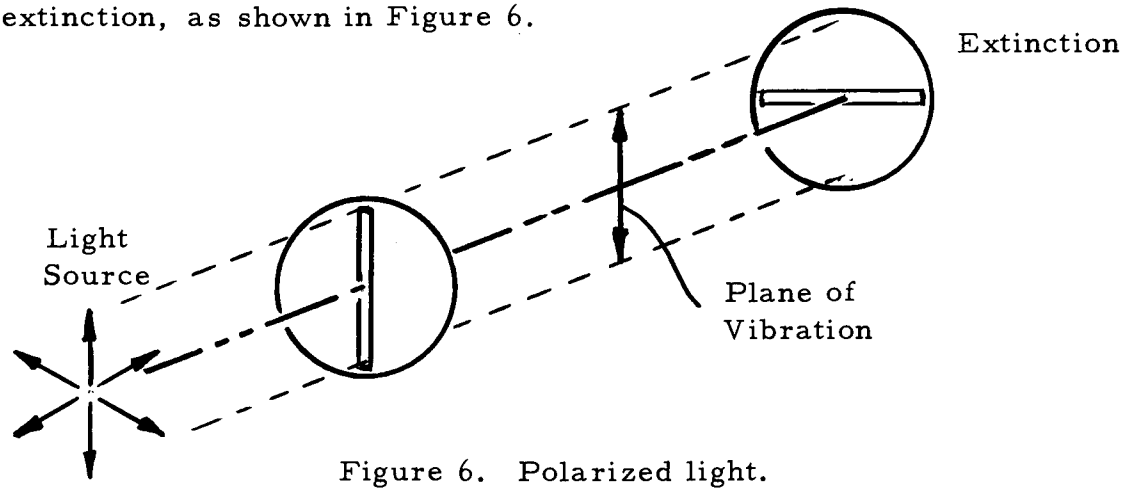

Figure 6. Polarized light.

Strain-Optic Effects

The index of refraction is a physical property of all transparent solids and is defined as the ratio of the speed of light in a vacuum to the speed of light in the solid. It is always less than unity and in a homogenous material is constant regardless of the direction of vibration of the light. Certain materials, notably plastics, are normally homogeneous but become heterogeneous when strained. The index of refraction for light vibrating in the direction of one principal strain varies from the index for light vibrating in the direction of the other. The fact that this difference of indices can be measured optically and related to strain is the basis for photoelastic theory. Further, it has been established (Brewster's Law) that the relative change in the index of refraction is proportional to the difference in principal strains. Thus,

$$(n_a - n_b) = K(\epsilon_a - \epsilon_b) \tag{10}$$

where n_i is the index for light vibrating in the direction of the principal strain ϵ_i (i = a or b).

K is the strain-optical coefficient which characterizes a physical property of the material.

Now consider Figure 7. A polarized beam of light P propagates through a transparent plastic of thickness t. The plastic is stressed such that a and b represent the axes of principal strain.

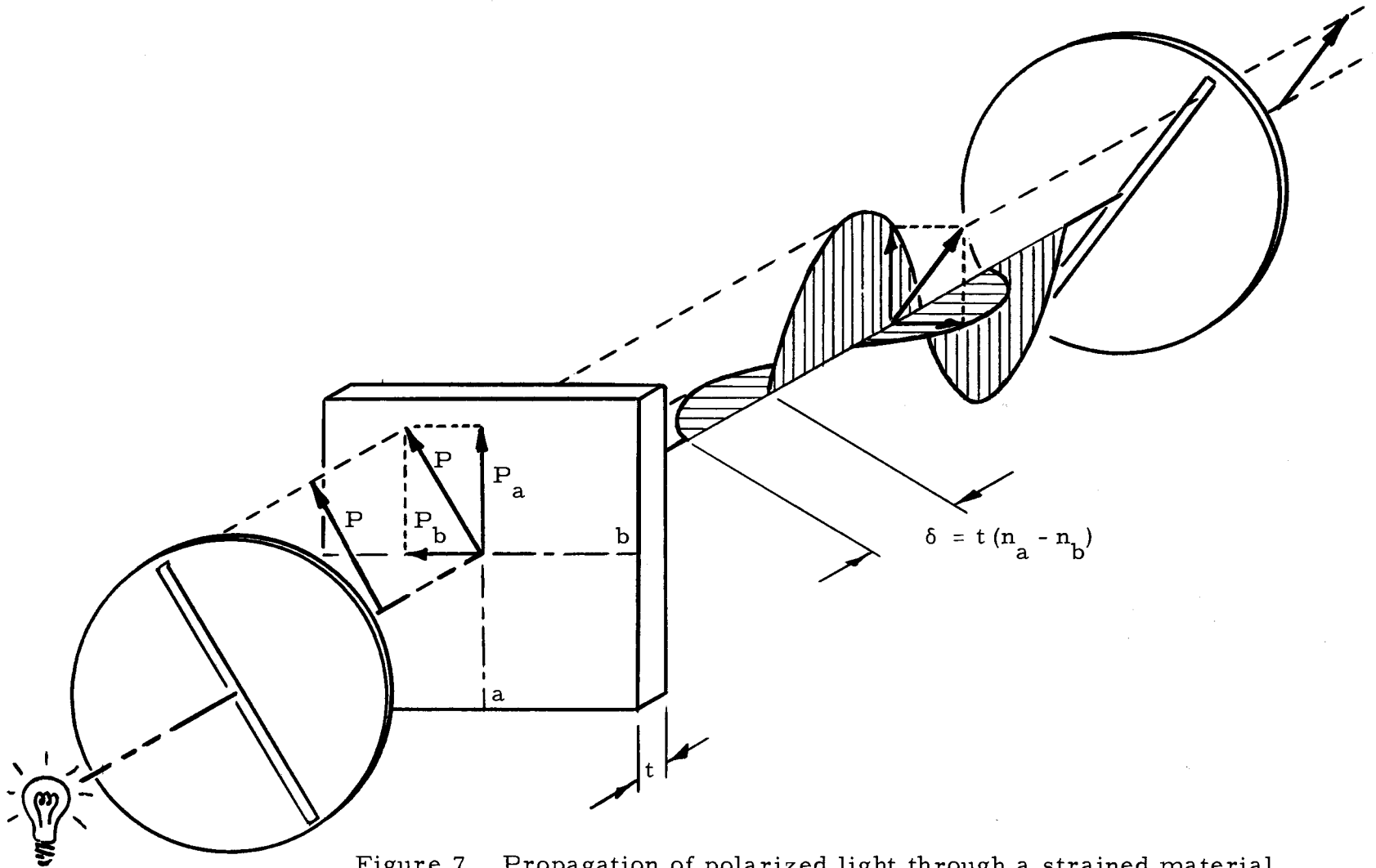

Figure 7. Propagation of polarized light through a strained material.

The vectors represent the amplitude and direction of vibration of the light waves. The light beam P can be visualized as two component beams P_a and P_b. If the speed of the light beam P_a in the plastic is V_a and the speed of P_b is V_b and if the time necessary for each to traverse the plastic is t/V then the relative retardation in units of length between P_a and P_b after they emerge is given by:

$$\delta = C\left(\frac{t}{V_a} - \frac{t}{V_b}\right) = t(n_a - n_b) \tag{11}$$

where δ is the relative retardation or physical distance by which the light beams P_a and P_b are out of phase.

C is the speed of light.

t is the plastic thickness.

V and n are the light velocity and the index of refraction as previously defined.

Combining Eqs. (10) and (11) results in Eq. (12).

$$\delta = tK(\epsilon_a - \epsilon_b) \tag{12}$$

The value of this expression will become apparent later.

Note that the second polarizing filter in Figure 7 no longer causes extinction as it did in Figure 6. The relative retardation has caused an effective vibration in a direction which will pass through the second filter.

Strain-Optic Effects in a Photoelastic Coating

Suppose that the back surface of the plastic in Figure 7 was made reflecting and the second polarizing filter was brought around in front as shown in Figure 8.

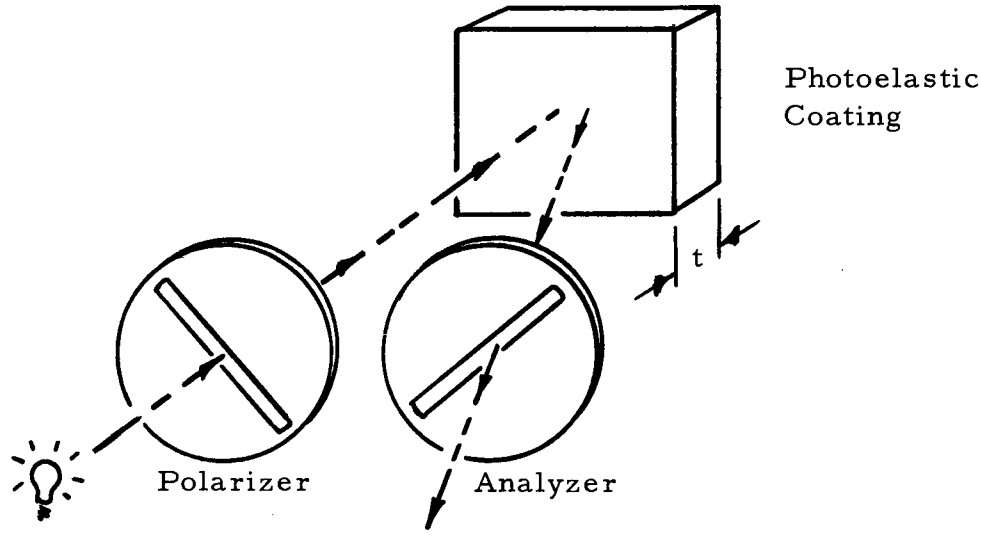

Figure 8. Light path for a photoelastic coating.

The effect is the same except that the length of the light path in the plastic is now twice the thickness. Thus, Eq. (12) becomes Eq. (13) for a photoelastic coating.

$$\delta = 2tK(\epsilon_a - \epsilon_b) \tag{13}$$

Determination of Principal Strain Directions

The last two sections have shown that when a plane polarized beam of light is traversing a photoelastic coating subjected to stresses, the beam can be visualized as two component beams aligned with the principal strain directions and propagating at different speeds. After emerging from the coating, the two beams are usually out of phase and will not recombine into another plane polarized beam vibrating parallel to the original beam. Rather, these emergent beams will contain vibrations in directions different from the original beam and will not be entirely extinguished by the second polarizing filter. However, if the first polarizing filter (the polarizer) has its axis aligned with a principal strain direction, then all light will be extinguished by the second polarizing filter (the analyzer). This fact is easy to see from Figure 7. If the plane polarized light beam P were in a direction of either a or b then all of P would propagate through the plastic at the same speed and emerge unchanged. Since the analyzer is oriented perpendicular to the polarizer and hence perpendicular to P, extinction would occur.

Applying the above principles to the problem of determining principal strain directions in a photoelastic coating is a simple matter. The coating is observed with a reflection polariscope (the name given to the combination of light source, polarizer, and

analyzer shown in Figure 8). Dark lines or areas called isoclinics appear on the coating which correspond to points at which the principal strain directions are aligned with the axes of the polarizer and analyzer. To find principal strain directions at other points on the coating, the polarizer and analyzer are rotated together until isoclinics appear at the points in question. The angle that the axes of polarization make with some reference direction is read directly from graduations on the polariscope. Figure 9 illustrates isoclinic extinction in a coating.

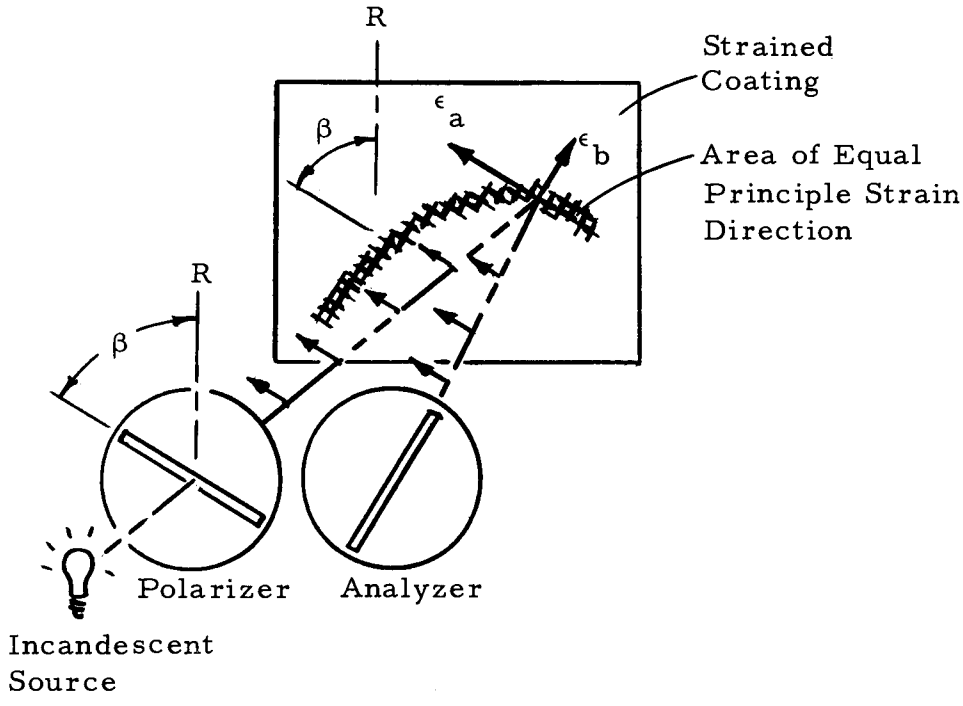

Figure 9. Isoclinic extinction in a photoelastic coating.

When principal strain directions are desired over an entire field, isoclinic patterns are usually photographed at many incremental settings of the polariscope.

Determination of the Principal Strain Difference

Second Mode of Extinction

Close examination of Figure 7 will reveal another way in which light traversing the plastic suffers complete extinction by the analyzer. Suppose that the principal strains along a and b are such that the relative retardation between beams P_a and P_b is exactly equal to one wavelength of the light. Figure 10 shows the light after emerging from the plastic for this case.

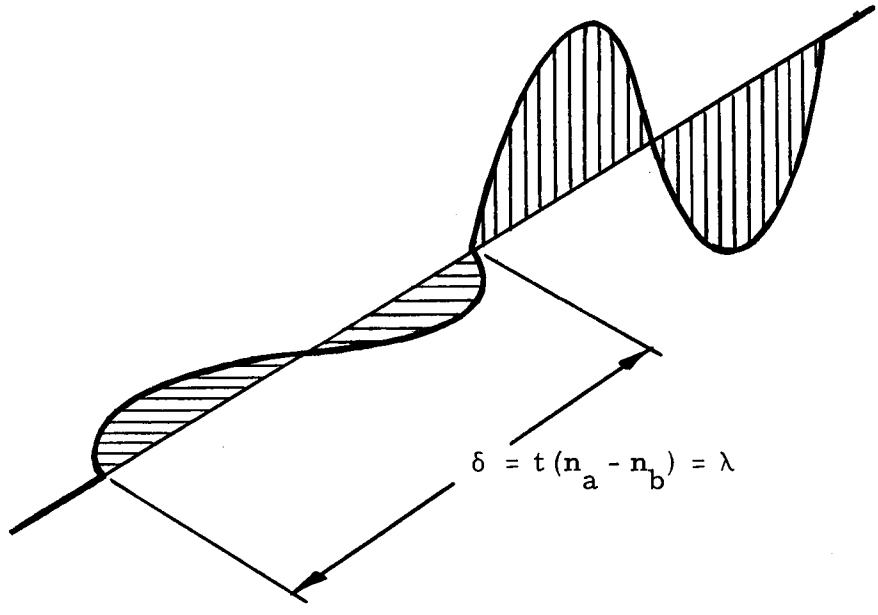

Figure 10. Retardation by one wavelength.

Since light is a continuous train of waves, the emergent light in Figure 10 will appear identical to the light beam P entering the plastic and will, therefore, be extinguished by the analyzer. Clearly, every instance in which the relative retardation is equal to an integral number of wavelengths (or zero) will cause an extinction by the analyzer. Mathematically, extinction occurs when:

$$\delta = m\lambda \tag{14}$$

where δ is the retardation.

m is an integer or zero.

λ is the wavelength of light.

This type of extinction is called an isochromatic fringe and is related to the principal strain difference in a photoelastic coating by Eq. (15), which represents a combination of Eqs. (13) and (14).

$$m\lambda = 2tK(\epsilon_a - \epsilon_b) \tag{15}$$

Thus the principal strain difference $(\epsilon_a - \epsilon_b)$ at a point on the coating may be computed from Eq. (15) by observing the order of retardation (m) and the color or wavelength (λ) being extinguished.

Wavelength of Extinction

The term "isochromatic fringe" implies a fringe of the same or equal color. When white light is used in a polariscope, the meaning becomes clear. Bands or areas of different colors appear on the

coating as illustrated by the photograph of a photoelastic disc under diametral compression in Figure 11.

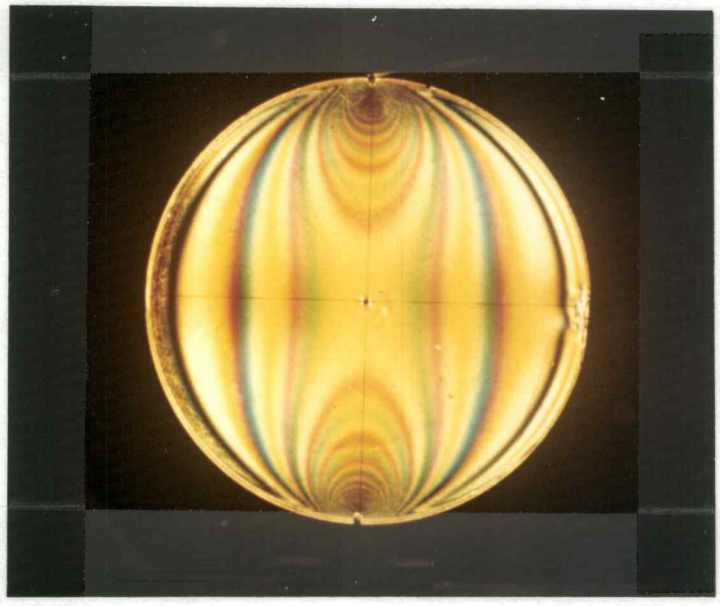

Figure 11. Isochromatic fringe pattern in a disc subjected to diametral compression.

Each band represents the color that remains when a single wavelength is removed from white light. For example, a band of red indicates that the color green has been extinguished from the incident white light. The wavelength of green which is about 4500 Å or 17.7 μin would be substituted into Eq. (15).

Order of Retardation

Observation of a red fringe is not sufficient information to assume that the retardation is 4500 Å. It could also be 9000 Å,

13000 Å, or m times 4500 Å, where m is the integral order of retardation. Two methods can be used to determine m.

With the first method, the coating is loaded slowly from zero so that the number of times a color appears at the point in question can be counted. This number will equal the order m for that color. This is evident from Eq. (15).

Since the principal strain difference $(\epsilon_a - \epsilon_b)$ must progress in a smooth manner from zero to its value at full load, then the order of retardation m must likewise progress in an orderly manner 0, 1, 2, etc.

The second method entails counting the number of times that the red fringe appears between the point in question and an isotropic point, i. e., a point of known zero principal strain difference such as a 90° corner free of fractions. Here again, in a strain field, the principal strain difference must change smoothly from zero to its value at the point in question. The order of retardation of any particular fringe is simply the integer attached to the fringe when fringes of the same color are numbered from zero at an isotropic point.

Determination of Individual Principal Strains

In the previous sections methods have been outlined for determining the principal strain directions and their difference. This is

often enough information to solve problems since the principal strain difference at a point is equivalent to the often needed maximum shear strain at that point. In addition, the stress situation along all free boundaries is completely defined because of the additional knowledge that the stress normal to a boundary must be zero. In the general case of an interior point, however, knowing the principal strain directions and their difference is not enough and it is necessary to determine the individual principal strain magnitudes. An experimental method known as the oblique incidence method is available for doing this. Mathematical and graphical techniques can also be used.

Oblique Incidence Method

By the use of the instrument schematically shown in Figure 12 which causes light to traverse a coating in an oblique path, additional information about the principal strains can be obtained.

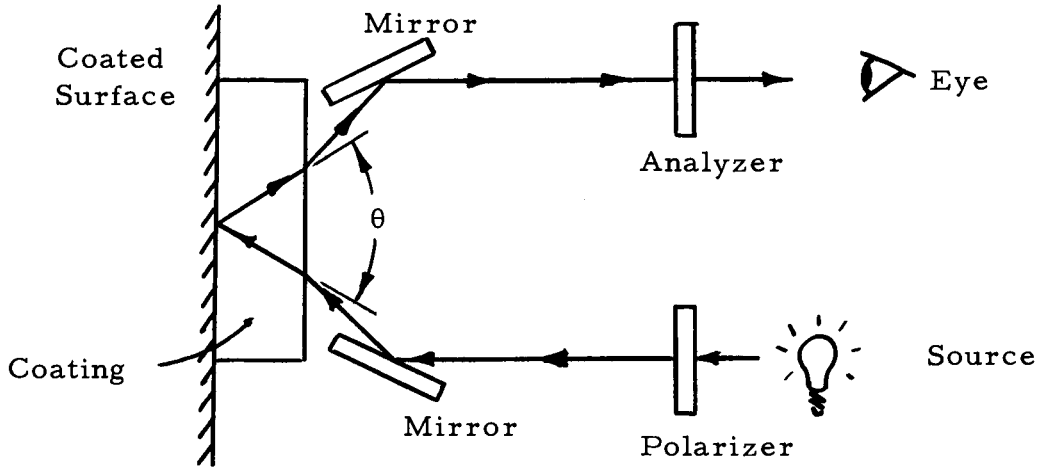

Figure 12. Oblique incidence.

An analysis of the light as it propagates through this instrument produces Eq. (16) which is similar to but independent of Eq. (15).

$$\delta_o = m_o \lambda = 2tK(A\epsilon_a - B\epsilon_b) \qquad (16)$$

where subscript o refers to oblique incidence

A and B are constants depending on the angle θ in Figure 12.

Together, Eqs. (15) and (16) can be solved for the individual principal strains ϵ_a and ϵ_b. Drucker (11) has presented a thorough discussion of this method.

Mathematical and Graphical Methods

A few such methods are available for determining the individual principal strains from photoelastic data. All involve trial and error, numerical integration, or graphical procedures and are usually laborious. Frocht (15) and Durelli (13) present these methods in detail.

Two Types of Polariscopes

Plane Polariscope

The polariscope discussed to this point has had the configuration shown in Figure 13.

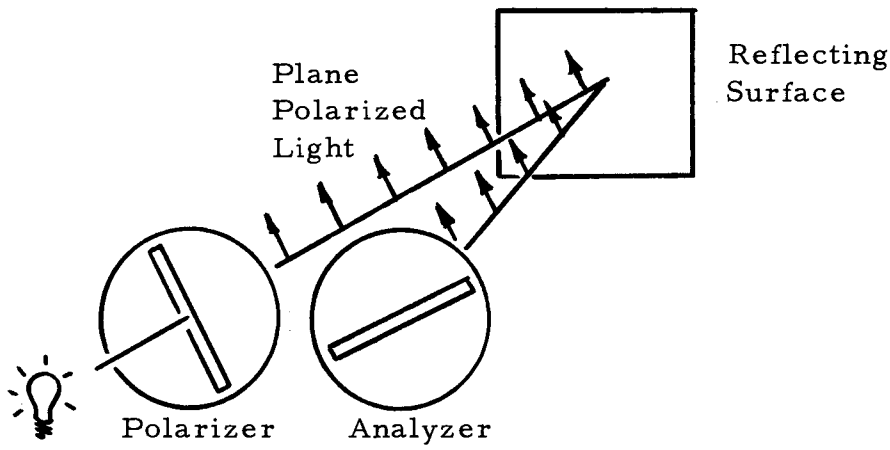

Figure 13. Reflection type plane polariscope.

The light propagating in this type (called a plane polariscope) is identified as plane polarized light because the vector representing the vibration of the light remains in a single plane. There are certain disadvantages with using a plane polariscope for all phases of a photoelastic investigation. One of these is the confusion between isoclinic extinction and isotropic extinction where the former is due to principal strain direction and the latter to zero principal strain difference. Both appear as dark lines or areas on the coating and are sometimes difficult to tell apart. Another of the disadvantages develops from using white light. After about four orders of retardation, the bands of color become indistinguishable from each other because as the retardation δ becomes large, it causes extinction of more than a single wavelength λ. This is seen from examination of Eq. (14) which is restated here.

$$\delta = m\lambda$$

where δ is the relative retardation between the beams of light propagating in a polariscope.

m is the integral order of retardation.

λ is the wavelength extinguished by the analyzer, i.e., the color extracted from the white light entering the polariscope.

Suppose $\delta = 24000\,\text{Å}$. Possible λ would then include $8000\,\text{Å}$, $6000\,\text{Å}$, $4800\,\text{Å}$, and $4000\,\text{Å}$ where the orders of retardation are $m = 3, 4, 5,$ and 6 respectively. Thus, four colors would be removed from the entering white light. The effect of this multiple extinction when δ becomes large is to give the fringes colors which cannot be identified easily. Monochromatic light is used to eliminate this problem since, then, there is only one wavelength to extinguish and fringes corresponding to this extinction appear dark. Here again, however, the problem of confusion with the dark isoclinic extinctions results.

Circular Polariscope

The circular polariscope provides a solution to problems mentioned in the previous section by simply eliminating isoclinic extinction while isochromatic and isotropic extinction remains. As with the plane polariscope the circular polariscope derives its name

from the nature of the light propagating through it. Circularly polarized light is produced by inserting a quarter-wave plate behind the polarizer as shown in Figure 14. A quarter wave plate is a heterogeneous transparent plate that behaves much like the stressed plastic in Figure 7. Light vibrating along one of its axes traverses the plate slower than light vibrating along the other perpendicular axis. The thickness of the plate is adjusted so that the relative retardation between the two beams as they emerge is exactly one-quarter of a wavelength, hence the name. The axes in the plate are labeled slow (s) and fast (f). If these axes are adjusted at 45^{o} to the polarizer, circularly polarized light (circular light) is generated. This designation comes from the fact that the vector associated with the light scribes a circle on a plane as the light wave propagates normal to the plane. Figure 14 demonstrates circular light generation.

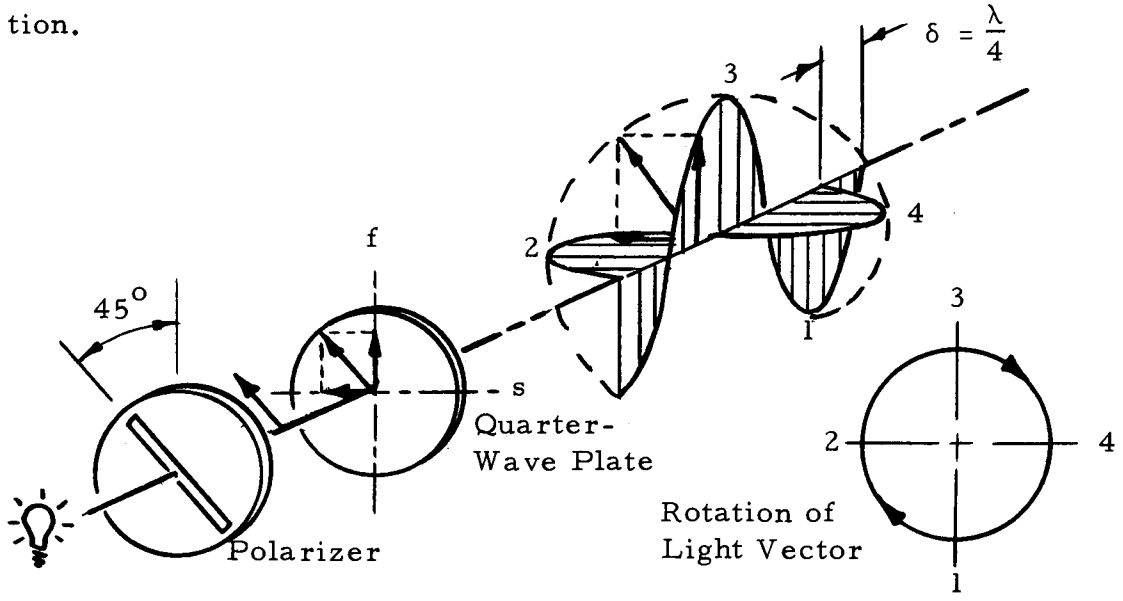

Figure 14. Circular light generation.

In a circular polariscope a second quarter-wave plate is inserted just before the analyzer to return the circular light to plane polarized light. A circular polariscope is shown schematically in Figure 15.

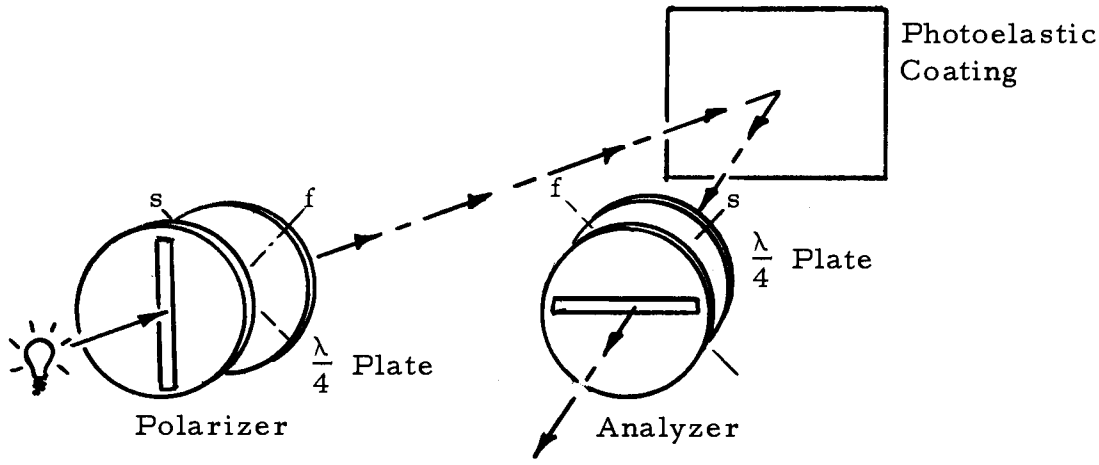

Figure 15. Reflection type circular polariscope.

How the addition of two quarter-wave plates to a plane polariscope eliminates isoclinic extinction is best explained by mathematically considering the propagation of light through a circular polariscope. This consideration is rather lengthy and omitted here. References (4, 14, 15) are recommended for a more complete discussion.

Basic Equation of the Photoelastic Coating Method

A mathematical study of the circular polariscope as mentioned in the previous section will also reveal that a rotation of the analyzer

relative to the polarizer will cause isochromatic extinction at fractional orders of retardation. This fact is expressed in Eq. (17).

$$(\frac{\alpha}{\pi} + m)\lambda = 2tK(\epsilon_a - \epsilon_b) \tag{17}$$

where α is the angle of analyzer rotation in radians.

This equation can be used to advantage. Suppose there is a point on a photoelastic coating at which the principal strain difference is desired and which lies between the integral isochromatic fringes m and m+1. Clearly, Eq. (15) is not applicable. To solve the problem, the analyzer is rotated relative to the polarizer so that the fringes are caused to move on the coating. By rotating the analyzer through a certain angle α, the integral fringe m can be made to move to the point in question. Noting α and m, the Eq. (17) can be solved for $\epsilon_a - \epsilon_b$. This is the basic equation of the photoelastic coating method and is usually written:

$$\epsilon_1 - \epsilon_2 = \frac{\lambda}{2tK}(m + \frac{\alpha}{\pi}) \tag{18}$$

where $\epsilon_1 - \epsilon_2$ is the principal strain difference to be computed at a point in the coating.

λ is the wavelength of extinction. With white light, λ corresponds to the wavelength extracted from the white light to give the color observed in the isochromatic fringe. With monochromatic light λ is

simply the wavelength of this light.

t is the thickness of the plastic coating.

K is the strain-optic coefficient of the plastic material.

m is the integral order of wavelength retardation, i. e., the isochromatic fringe order at the considered point.

α is the rotation of the analyzer relative to the polarizer in radians.

Eq. (18) is often written in the form of Eq. (19).

$$\epsilon_1 - \epsilon_2 = f\left(m + \frac{\alpha}{\pi}\right) \tag{19}$$

where $f = \frac{\lambda}{2tK}$ is called the strain sensitivity and can be thought of as the principal strain difference necessary to produce one fringe in the coating. It has units of μin/ in/ fringe and is usually specified by the manufacturer.

Reinforcing Effects of Photoelastic Coatings

The addition of a photoelastic coating to a structural member will increase the strength of the member to some degree, and this increase will be reflected in the data obtained from photoelastic measurements. Zandman and others (9, 12, 33, 46, 53) have made extensive investigations of this reinforcing effect and have developed

relationships for determining its effect on the photoelastic data taken from various types of experimental problems. There are four ways in which the so-called reinforcing effect can contribute to errors in photoelastic data.

1. Structure is stiffened because of additional stiffness of coating.
2. The addition of the coating can cause a disturbance in the stress distribution.
3. The photoelastic reading is averaged through the thickness of the coating.
4. Different Poisson's ratios between the coating and the structure cause the coating to induce a traction on the surface of the structure.

The first is the most obvious type of reinforcing and is dependent only on the relative stiffnesses of the structure and coating.

The second and third types are illustrated by the example of a plate in bending shown in Figure 16.

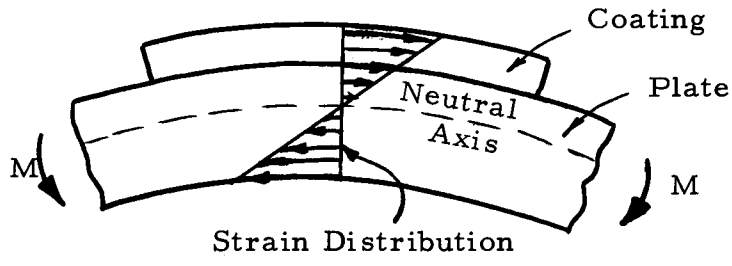

Figure 16. Plate in bending with coating.

The neutral axis has been shifted as a result of the unsymmetrical application of the coating. Further, there exists a strain gradient through the thickness of the coating. The photoelastic method will actually measure the average of this gradient which will not be the same as the strain on the surface of the structure. These two effects are entirely negligible in almost all problems except those where the thickness of the structure is of the same order as the thickness of the coating.

The fourth type of reinforcing caused by the difference in Poisson's ratios between structure and coating is demonstrated by a coated tensile specimen subjected to uniaxial tensile stress. When the Poisson's ratios differ, the lateral contractions due to Poisson's effect in coating and specimen also tend to differ. Since the strain of both coating and specimen must be identical at their interface, each must exert a traction on the other. This traction is identical to applying a lateral stress on the tensile specimen and will distort the photoelastic data.

The following correction factor was developed by Zandman (53) to account for the stiffness reinforcing and the Poisson's ratio effect, i.e., the first and fourth of the above types of reinforcing.

$$C = \left[1 + \frac{t_c E_c}{t_s E_s} \frac{(1 + \nu_s)}{(1 + \nu_c)} \right]^{-1} \tag{20}$$

where c designates coating.

s designates structure.

t thickness.

E modulus of elasticity.

ν Poisson's ratio.

and where

$$(\epsilon_1 - \epsilon_2)_{actual} = \frac{(\epsilon_1 - \epsilon_2)_{observed}}{C}$$

This correction factor was developed for isotropic structures but Stieda (40, p. 356) shows that it applies equally well to orthotropic structures when they are subjected to uniaxial stress parallel to an elastic axis.

The correction factors applying to general cases of biaxial stress in orthotropic structures are considerably more complex. Since the properties of stiffness and Poisson's ratio will vary significantly with direction on the surface of an orthotropic material, the correction factors for a general strain field will also vary at each point according to the directions of the principal strains. Clearly, applying correction factors to coatings on orthotropic materials can be a laborious point-by-point procedure. The difficulty is compounded with wood because wood has a relatively low stiffness and a high variability of elastic properties with direction. Stieda (40, p. 356) has presented general rules and equations for the application

of correction factors to wood. Figure 17 illustrates the difference between correction factors for steel, wood parallel to grain, and wood perpendicular to grain for various thickness ratios (coating to structure).

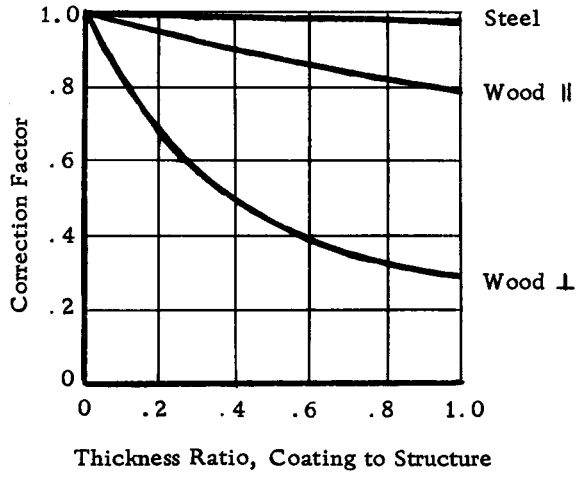

Figure 17. Reinforcing correction factors due to Stieda.

The curves in Figure 17 were computed from Eq. (20) using typical values for the elastic constants.

It is apparent from Figure 17 that as the thickness ratio approaches zero, so do all reinforcing effects. Ideally, a very thin coating is desired so that correction factors may be neglected. Other criteria must be considered, however, before a particular coating thickness is selected.

Coating Selection Principles

Coating selection is an important part of the photoelastic method and because of the great advances in the development of epoxy plastics in recent years, a wide selection of coating properties is available. There are four criteria for choosing the proper coating for a particular problem.

1. Strain sensitivity.
2. Reinforcing effect.
3. Accuracy required.
4. Temperature environment.

Strain sensitivity is measured by the strain sensitivity coefficient previously defined.

$$f = \frac{\lambda}{2tK} \tag{21}$$

It is the principal strain difference required to produce a single isochromatic fringe, i.e., first order extinction of the wavelength λ. A lower value of f indicates that more fringes will be observable for a given strain difference. Decreasing λ by using appropriate filters, or increasing the strain-optical coefficient K by selection of plastic, or increasing the coating thickness will lower the value of f. A choice must be made according to the expected level of strain. A high level of strain, for example in the plastic region, will require

a higher (less sensitive) value of f than will a low level. The accuracy with which the polariscope used can measure high fringe orders and fractional fringe orders will also have a bearing on what strain sensitivity will be required.

While an increase in the strain-optic coefficient (K) and the thickness will increase sensitivity, it will also increase the reinforcing effects. This results first because increase in K is found to correlate with an increase in the modulus of elasticity of the coating material and second because the stiffness of a coating varies directly its thickness. A compromise must be made after considering the particular problem.

The accuracy needed is an important economical consideration because high photoelastic precision requires high quality coatings at correspondingly higher cost. Common sense will dictate the coating that should be used.

Environmental temperatures are important for some applications. In most plastic coatings the strain-optic coefficient (K) is independent of temperature over a certain range of temperatures but becomes temperature dependent outside the range. This must be considered when a test is to be performed at elevated temperatures.

After consideration of the selection principles as they apply to a particular problem, a final choice must be made between the coating materials available. The manufacturers of photoelastic

coating materials, notably Photolastic, Inc., all provide the mechanical, optical, and temperature properties of their products on request.

Summary

The plane polariscope is used to find the isoclinics. An isoclinic is an extinction or dark area on the coating corresponding to the locus of points having the same principal strain directions. The directions that the principal strains have in a particular isoclinic are given by the orientation of the polarizer and analyzer assembly. To find the directions of principal strain at a point, the analyzer and polarizer are rotated together until an isoclinic appears at the point. The directions of the principal strains are then read directly from the polariscope. White light is used so that contrast between isoclinics and isochromatics is maximum.

The circular polariscope is used to find isochromatic fringes. An isochromatic fringe is an area of constant color on the coating which corresponds to the locus of points having the same principal strain difference. The magnitude of the principal strain difference is determined by observing the wavelength of light extinguished by the strain-optic effect and by observing the isochromatic fringe order. Eq. (19) is used for this computation. Isoclinic extinction is eliminated in the circular polariscope.

The oblique incidence method or various mathematical techniques can be used to determine the magnitudes of the individual principal strains if they are required.

Reinforcing effects of the coating on the structure coated are often significant and photoelastic data obtained should be corrected for them.

Coating selection is important and must be considered with respect to the needs of each individual problem.

V. TESTING PROCEDURES

Comparative Test Procedures

Test Objectives

Four tests were made on 12 nominal two-by-four inch Douglas Fir beams in order to compare results obtained from photoelastic coating data with results from standard deflection measurements and strain gage readings. There were three specific objectives of the tests. First, the modulus of elasticity (E) for each beam was computed from the results of each different test. An indication of the accuracy of the photoelastic coating method applied to wood was determined by comparing these E values. Second, the strain distributions in the beams determined by the coating method were compared with the distribution predicted by strain gages. Finally, the limitations and peculiarities of the coating method applied to wood were evaluated.

Test Specimens

Kiln-dry Coast Type Douglas Fir specimens were selected for tests. Six 90 inch finished two-by-fours were cut in half to yield six end-matched pairs of specimens 45 inches long. These 12 specimens were straight grained and free of defects. The faces of

the specimens were in general not parallel to the radial and tangential directions of the wood.

The cross-sectional dimensions of each specimen were measured with a micrometer. Five measurements were taken of each dimension and these were averaged to obtain the final value. Table 1 (p. 119) lists the dimensions of each specimen with the associated moments of inertia and other physical constants.

The specimens were identified as shown below.

A-1, A-2, B-1, B-2, ..., F-1, F-2

The same letter designation indicates end-matched specimens cut from the same 90 inch board.

General Testing Apparatus

All flexure tests were performed on a Baldwin BLW universal testing machine using a 6000 lb. maximum load range. Fixtures were devised to apply mid-point loading and third-point loading over a span of 39 inches with rollers used at supports and loading points to assure vertical loads. Schematic loading diagrams are shown in Figure 18; photographs of the third-point loading fixture in the testing machine appear in Figures 21 and 25.

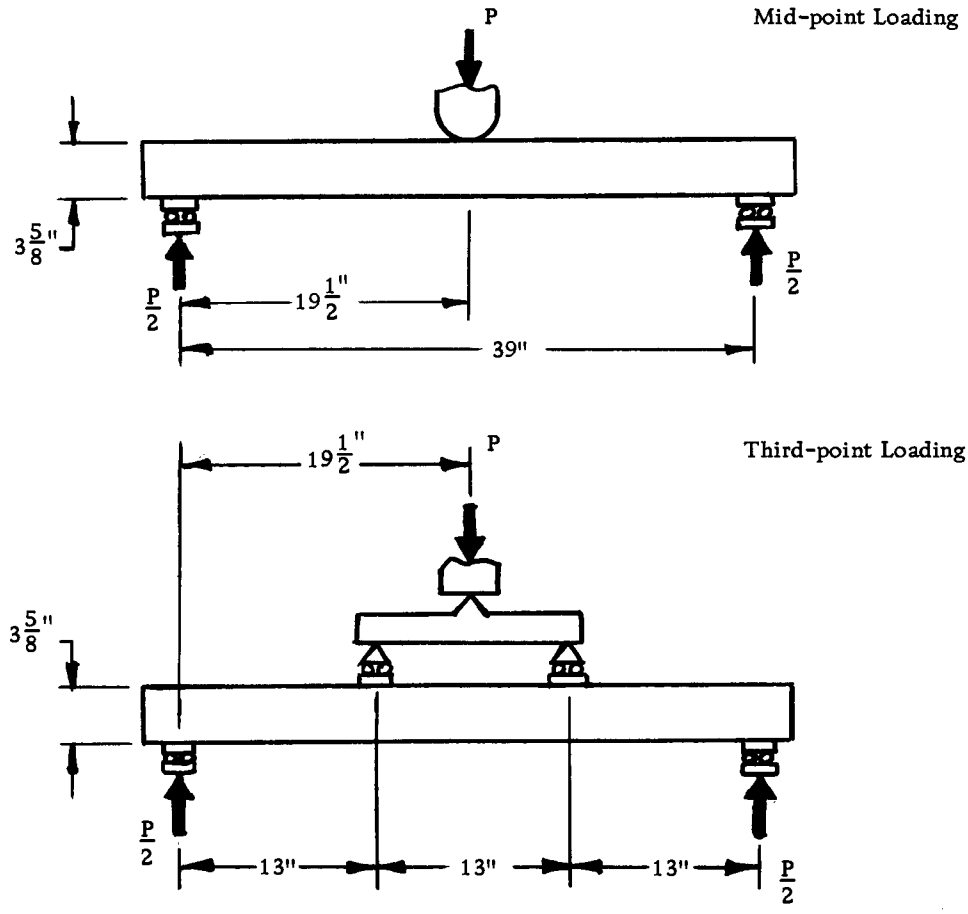

Figure 18. Loading diagrams.

Deflection Tests

Special Apparatus. A Baldwin deflectometer which utilized a linear variable differential transformer coupled with a Baldwin recorder was used to measure mid-point deflection of the test specimens. The load indicator was also coupled with the recorder so that the final output was in the form of a load-deflection curve. The deflectometer output was calibrated by comparison with a Starrett dial gage before and after each test period. The dial gage

was checked against a micrometer. The load recording function was calibrated by comparison with the load indicating scale on the testing machine.

Testing Method. Deflection tests were performed on each specimen under third-point loading and mid-point loading. The American Society for Testing Materials standards for flexure tests of small clear timber specimens were followed with the following major exceptions: 1-5/8" x 3-5/8" x 45" specimens were tested instead of the recommended 2" x 2" x 30" specimens and third-point loading was used in addition to mid-point loading. A loading span of 39" was used instead of 28" and the rate of loading was slower than the recommended rate. Since non-destructive tests were obviously necessary, the test loads were not increased to destruction as required by the standard but were kept just under the maximum working load recommended by the Wood Handbook (47, p. 156-159). Computations were based on a maximum working stress of 3020 psi for clear, dry, medium-grained coast type Douglas Fir. Deflections of the bottom of each beam at mid-span were measured relative to the supports whereas the standard specifies that deflections of the beam's neutral axis shall be measured.

Each specimen was tested under mid-point and third-point loading on two different days a week apart. The specimens were brought to full load several times before any measurements

were taken in order to seat the beams to the supports. A load-deflection curve was obtained for each loading and a total of four of these curves was obtained for each specimen.

Strain Gage Tests

The procedures for the strain gage tests were identical to those for the deflection tests except that only third-point loading was used and strain gage measurements were substituted for deflection measurements.

Special Apparatus. This included a Baldwin-Lima-Hamilton strain indicator and switching unit and 48 SR-4 bonded wire, paper backed, electric resistance strain gages made by BLH Electronics, Inc. The strain indicator incorporates a bridge circuit which accurately measures the strain gage resistance and is calibrated to read out in units of strain. The switching unit enables the investigator to rapidly measure strain in a number of gages with the same indicator without changing wires for each gage. The strain gages used were of type A-5-1 (1/2 inch gage length) and A-3 (3/4 inch gage length) both with resistances of about 120 ohms.

Use of Strain Gages on Wood. The application methods outlined by the U. S. Forest Products Laboratory (51) were used. These methods differ from those for mounting gages on metallic surfaces in two ways:

1. The surface is cleaned by sanding with fine sandpaper instead of by using solvent.
2. The wood surface is prepared by applying a thin coat of adhesive and allowing it to dry before the gage is cemented in place instead of by using metal conditioners.

Temperature compensation for strain gages on wood is more critical than for gages on metallic materials. When a gage is being used, heat is electrically generated from the current used to measure resistance. To compensate for changes in resistance due to this heating and ambient temperature changes an identical gage is put in one arm of the bridge circuit and is subjected to the same environmental conditions but is not strained. The temperature effects in the gages cancel each other so that only resistance changes due to straining are apparent. These compensating gages are especially necessary on wood because wood is a poor conductor of heat and, therefore, gages applied to wood will become warmer and will stay warm longer than gages applied to metal. Also, since heat conduction in wood is dependent on type of wood and grain direction, the compensating gage must be mounted identically to the active gage if the two gages are to have the same temperature history. It should be noted further that each active gage must have its own compensating gage. If an attempt is made to use a single or common compensating gage with number of active gages through a

switching unit, the compensating gage will be continuously energized and thus will reach its equilibrium temperature whereas an active gage will only be periodically energized and usually will not have reached its equilibrium temperature when its resistance is measured. This phenomenon is called thermal drift and is characterized by a drifting of the strain indicator when a dormant active gage is switched into the circuit with a common compensating gage. The purpose of the compensating gage is obviously defeated if it is not at the same temperature as the active gage. It is possible to wait until the active gage reaches equilibrium before taking readings but this is an undesirable waste of time. It is usually more convenient to use a separate compensating gage for each active one so that both incur precisely the same time-temperature conditions. Thermal drift is negligible for gages mounted on metal because heat is conducted away from the gages at such a rate that temperature equilibrium is reached almost immediately by an energized gage.

Testing Method. All specimens were again tested under the third-point loading illustrated in Figure 18. Four strain gages were mounted on the top and bottom surfaces of each specimen as shown in Figure 19. The gages were centered on the top and bottom faces with respect to specimen width.

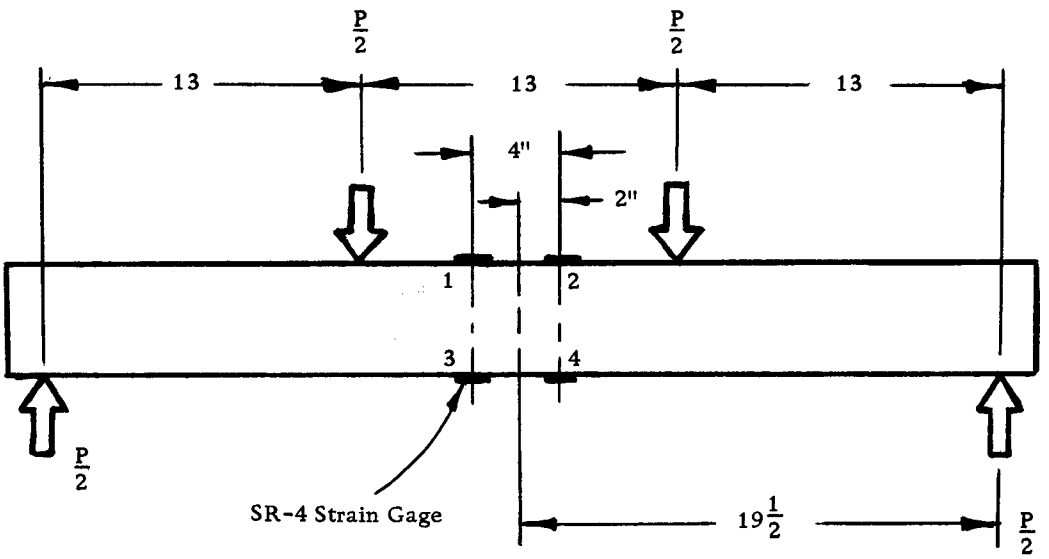

Figure 19. Strain gage mounting positions.

The tests were conducted on two different days as was done with the deflection tests. On both test days each specimen was loaded twice to P = 1500 lb. or an approximate maximum fiber stress of 2900 psi. Strain gage readings were taken at intervals of 250 lb. loading and 250 lb. unloading on the first test day and at intervals of 500 lb. loading and 500 lb. unloading on the second test day. The interval was changed because data from the first test showed that the additional readings were not necessary.

Individual temperature compensating gages identical to and of the same lot number as the active gages were provided. The procedure was to use the gages on one specimen as compensating gages for the active gages on the specimen being tested.

Photoelastic Coating Tests

Special Apparatus. A reflection polariscope, a 35 mm camera with film, and a monochromatic filter were required for the photoelastic tests. The reflection polariscope was designed and built using circular fluorescent lamps as suggested by Slot (37). The essential characteristics of the polariscope are shown in Figure 20.

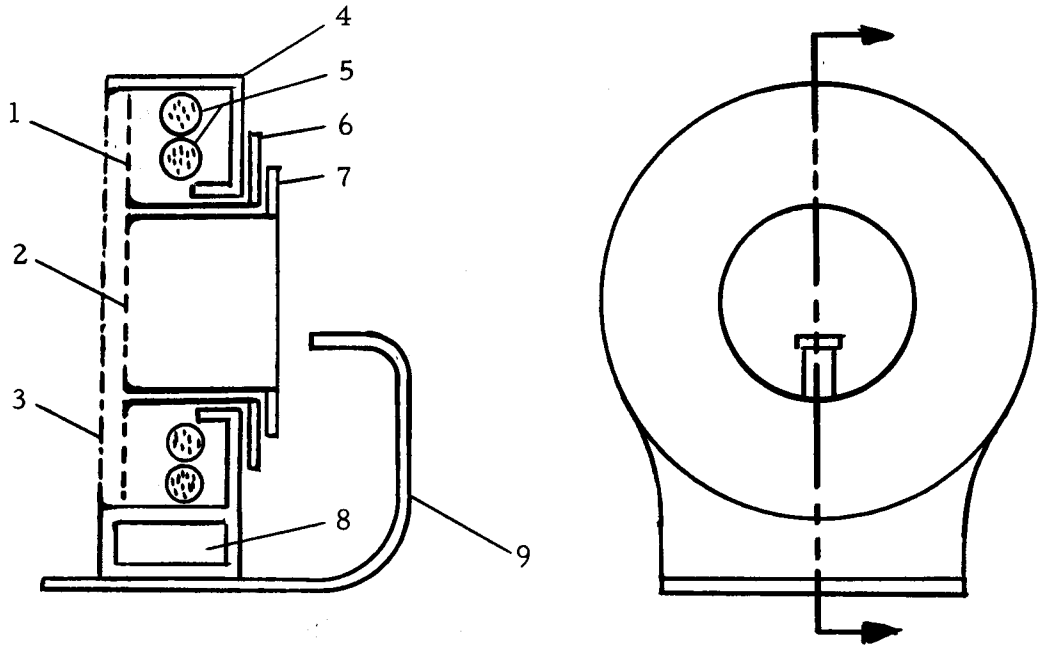

(1) Annular polarizer fixed to outer concentric cylinder.
(2) Analyzer fixed to inner concentric cylinder.
(3) Detachable quarter wave plate fixed to housing.
(4) Housing.
(5) Circular fluorescent lamps.
(6) Polarizer ring knob fixed to outer concentric cylinder and controlling rotation of polarizer.
(7) Analyzer ring knob fixed to inner concentric cylinder and controlling rotation of analyzer.
(8) Compartment housing lamp ballast and fan.
(9) Support for 35 mm camera.

Figure 20. Diagram of reflection polariscope constructed for tests.

A 35 mm Honeywell Pentax camera was used to record data on Kodak 35 mm Tri-X Pan film, ASA speed 400. A filter used to obtain monochromatic light of a very narrow band centered on the 11.35 μin wavelength was mounted over the lens of the camera. The polariscope and camera are shown ready for testing in Figure 21.

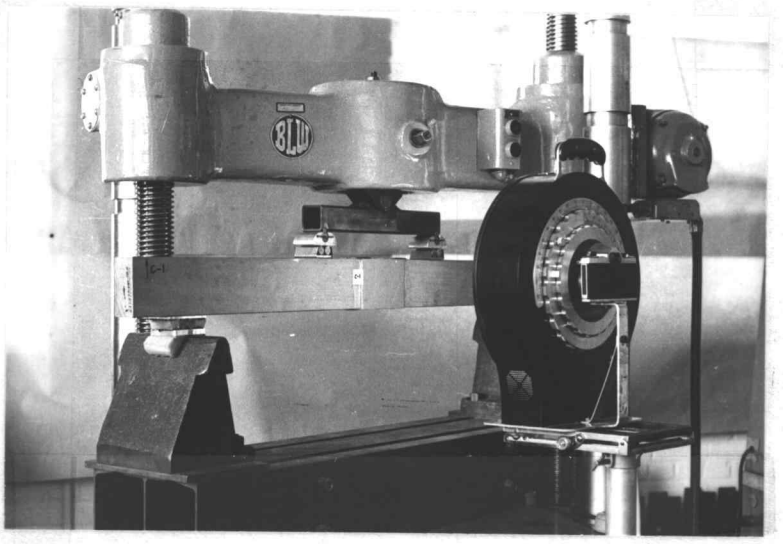

Figure 21. Photoelastic test set-up.

Coating Selection. Coating sensitivity and reinforcing effects were held to be the basic criterion applying to these tests. It was felt that about two observable isochromatic fringes in both compression and tension would give satisfactory results and from this requirement the minimum acceptable sensitivity was approximated. By

assuming a modulus of elasticity (E_L) for wood of 2×10^6 psi, the maximum fiber strain in the specimens at maximum load (P = 1500 lb.) was shown to be about 1450 μin/in. Assuming a Poisson's ratio of 0.3, the maximum principal strain difference in the extreme elements of a specimen's face was computed to be 1880 μin/in. Since the sensitivity is defined as the principal strain difference necessary to give a single fringe it was obvious that a sensitivity of 940 μin/in/fringe would be required for two fringes. Having this minimum sensitivity requirement, it was convenient to go to a manufacturer's table relating sensitivity and thickness for the materials available. A table from Photolastic, Inc. was obtained for this purpose and the coating material described on page was selected.

A number of experiments performed with this material previous to the actual tests demonstrated adequate sensitivity. Dahlke (6) also reported favorable results from his experiments with this coating.

Cutting and Mounting of Coatings. From three 10 inch square sheets of the coating material, twelve 5.00 x 1.63 inch plates were roughed out with a high speed band saw and finished to size with a high speed router designed especially for cutting photoelastic materials without causing residual stresses. These plates were then mounted on the specimens as shown in Figure 22.

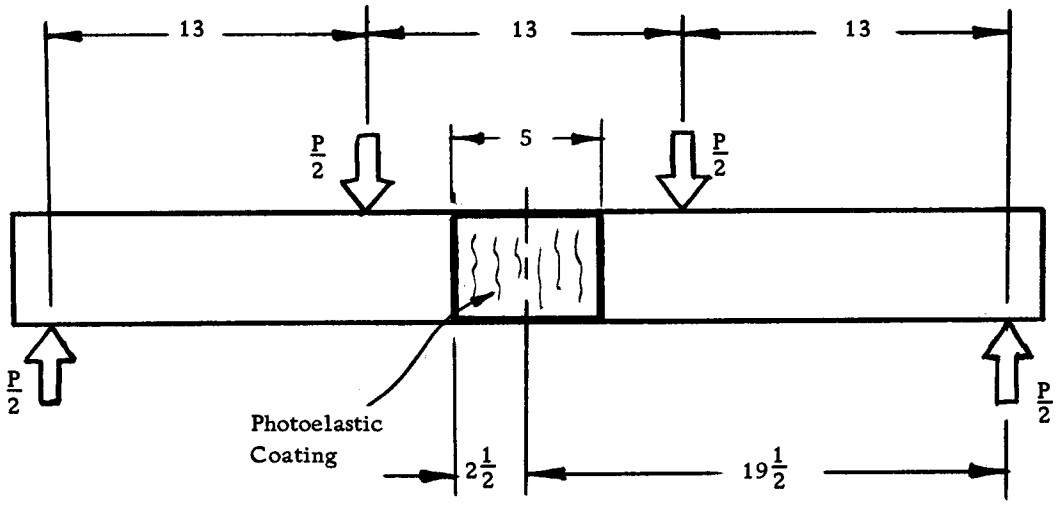

Figure 22. Coating position on tests specimens.

Figure 21 shows a photograph of the coating material cemented to a specimen ready for testing. No special techniques were required to cement the coating material to wood. The process differed from application to metallic surfaces only in the respect that the wood surface was sanded clean and smooth with fine sandpaper. The manufacturer's application instructions were followed closely.

Testing Method. The 12 specimens were again subjected to third-point loading as shown in Figure 18. Each specimen was loaded to P = 1500 lb. and two photographs recording the whole-order and half-order isochromatic fringes were taken. An analysis of these photographs indicated that for many of the beams there was an upward shift of the strain pattern caused by previously unnoticed residual strains in the coatings. The residual strains were uniform over the coating as evidenced by the fact that there was no fringe

pattern observable on the coating prior to loading in the initial tests. A uniform residual strain has the effect of adding (or subtracting) a constant to all strain readings taken from the coatings. For the case of the beams in pure bending the residual strain causes an apparent shift in the neutral axis since the points of zero strain in the coating occur at points where the strain in the beam induced by loading cancels the residual strain. To correct the original data, new tests were made on the beams and the residual strains were eliminated by carefully adjusting the polariscope to read zero strain prior to loading. Of course this adjustment could have been made in the initial tests had the residual strains been more apparent. Substantial residual strains can be present, however, before the effect is noticed because of the slow change of coating color from black to gray to yellow for the initial strains. The difference between the black and gray is very slight and a gray coating with residual strains will not be detected unless the investigator is aware that the problem might exist. For the new tests, direct measurements of the fringe locations on the coatings were made with a small scale and from this data the location of the true neutral axis was determined. By comparing the true neutral axis location with the location predicted by the first tests the residual strain in each beam was computed and the original test data was corrected accordingly. Another way of handling this problem would have been to retest all specimens taking precautions

to eliminate the effect of residual strains. It was not desirable to do this for the following reason. By the time that the residual strain problem had been discovered, considerable time had passed since strain gage and deflection tests were made. Since strength properties of wood are affected by seasonal humidity changes the modulus of elasticity for the specimens had certainly changed so that the results from completely new tests could not be validly compared to results from strain gage and deflection tests. On the other hand, changes in humidity will not affect the location of the neutral axis and it was convenient to measure this parameter in new tests for use in correcting original data.

Since the principal strain directions were known from the loading arrangement, isoclinic fringe photographs were unnecessary. Figure 21 shows the apparatus in position for testing.

Laminated Wood Test Procedures

Test Objectives

The objective was to use the photoelastic coating method to investigate a stress analysis problem in wood concerning the stress distributions around the joints in boards constructed of laminated, butt joined, 1/4 inch veneer. The specific questions which were investigated are listed below.

1. At what distance must butt joints be separated to eliminate the interaction of their individual stress concentrations?
2. To what extent does the size of the gap at a butt joint effect the stress concentration caused by the joint?
3. To what extent does a well glued butt joint reduce the stress concentration caused by the joint?
4. Is there a significant difference between the stress concentrations caused by a butt joint in compression and a butt joint in tension?
5. What is the approximate magnitude of the stress concentration caused by a butt joint?

Test Specimens

Five specimens having various types of butt joints were obtained from the Weyerhaeuser Company in Longview, Washington. All five were constructed of laminated 1/4" Douglas Fir Veneer. An edge view of the specimens is shown in Figure 23 and the butt joint descriptions, cross-sectional dimensions, and other data for the specimens are given in Table 2 (p. 120).

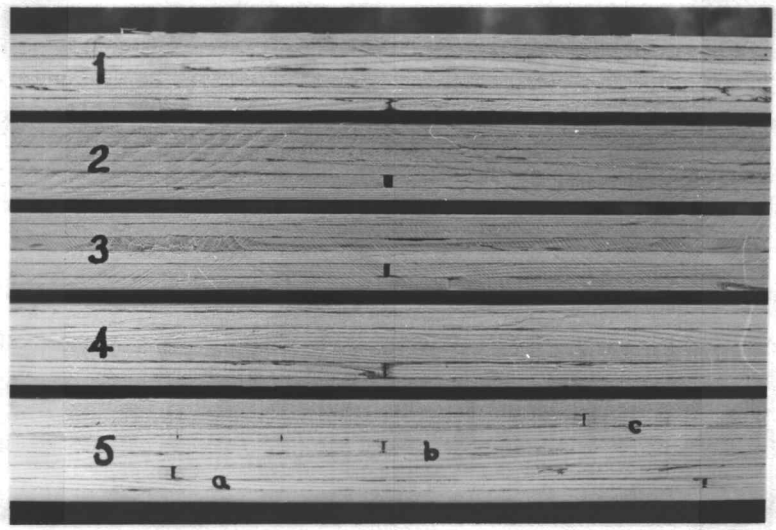

Figure 23. Photograph of laminated test specimens showing butt joints.

Testing Method

The laminated specimens were tested under third-point loading with the same machine and fixtures used in the previous comparative tests. The portion of each specimen containing the butt joint was subjected to the pure bending type of stress distribution found between the loading points. Figure 24 illustrates a specimen under load.

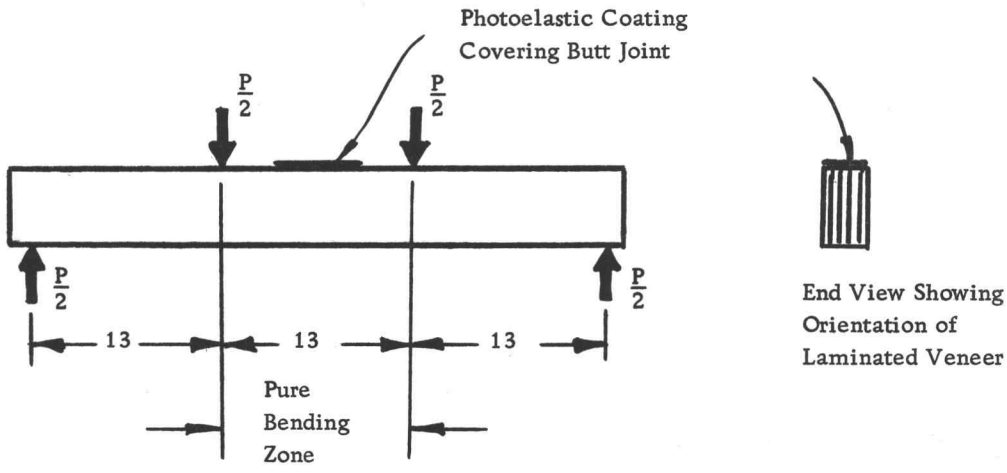

Figure 24. Placement of coating on laminated test specimens.

To investigate the strain distribution in the area of a butt joint, a plate of coating material was cemented over the joint as shown in Figure 24. A rubber packing material was used to fill gaps in joints so that the coating adhesive would not flow into the gaps and strengthen them. The coating material and methods of application were the same as those used in the previous comparative tests. Tests were run on specimens with the coated surface in both tension and compression. Figure 24 shows the coated surface in a constant compression field. The specimens were inverted to obtain a constant tension field.

In order to view the coated surface at normal incidence and still make use of the testing arrangement shown in Figure 21, a first surface mirror was used. The mirror was mounted so that it could

be adjusted to reflect the top or bottom faces of the specimens. Figure 25 shows the mirror positioned in the testing machine for reflecting the tension face of a specimen.

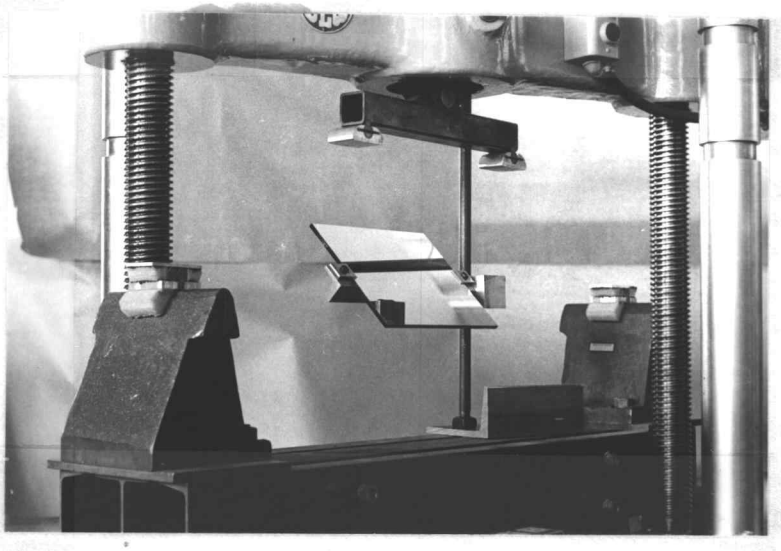

Figure 25. Photograph of first surface mirror in position to reflect bottom (tension) face of laminated test specimen.

Two data photographs were taken for each specimen: one of the butt joint in a tension field and one of the joint in a compression field. In each case the load was sufficient to cause the stress in the extreme fibers to be the approximate maximum working stress of 3020 psi. Computations for determining this load are given on page 126.

VI. DATA REDUCTION

Humidity and Temperature Effects

Humidity

Because wood is hygroscopic, humidity affects its moisture content and the moisture content in turn affects strength properties. Dry wood is considerably stiffer and stronger than wet wood. When the results of one test are to be compared with results from another, the investigator must be sure that they are corrected to the same moisture content conditions or differences may cause comparisons to be invalid.

While humidity is related to the moisture content of wood, the relationships hold only when the wood is in moisture equilibrium with the atmosphere. The time required for wood to come to equilibrium is considerable and depends on the thickness of the wood and the magnitude of the humidity change. Certainly, fluctuations of moisture content will not follow daily fluctuations of humidity. In fact it can be assumed that fluctuations of humidity over a period of four or five days will affect the moisture content in a two-by-four only slightly.

It was assumed for these tests that humidity fluctuations during the testing period were not large enough to cause an appreciable

change in moisture content of the specimens. As a basis for this assumption, a humidity record for the two weeks preceding each test date was obtained. While the record showed considerable hourly and daily change, the average for each two week period prior to a test was within 15% relative humidity of the others. A change of 15% relative humidity corresponds to an equilibrium moisture content change of about 3% and from the work by McBurney and Drow (24) this corresponds to a change in the modulus of elasticity of about 1.8%. Since this was the maximum error considered possible by neglecting humidity changes, correction factors were assumed unnecessary. As a check on this assumption, identical tests on the 12 specimens were made on different days. The tests were separated by one week for which the average relative humidity was about 15% higher than for the week preceding the initial test. The modulus of elasticity for each beam was computed from both tests and no average significant increase or decrease in the moduli for the beams was detected.

Temperature

According to the Wood Handbook (47, p. 89) the strength properties of wood are decreased (increased) by approximately one-third to one-half of one percent for every degree the wood's temperature increases (decreases) from 70°F. As with humidity the results

of tests made at different temperatures must be corrected to the same temperature before comparisons can be made.

For these tests temperature effects were considered negligible because laboratory temperatures during all tests were nearly constant at about $70^{\circ}F$.

Deflection Data Reduction

Data were obtained from mid-point loading and third-point loading flexure tests in the form of load-deflection curves. These curves were very nearly linear except for a short initial segment. The slope of the linear portion was recorded and used to compute the modulus of elasticity (E) for each specimen. (In the following chapters E will denote the modulus of elasticity in the longitudinal direction and the subscript L normally used will be omitted.) Shear deflection of the specimens is a significant part of the total deflection and was computed. In all calculations the wood was assumed to be orthotropic.

Shear Strain Energy

Consider the small element shown deformed by a shear stress τ.

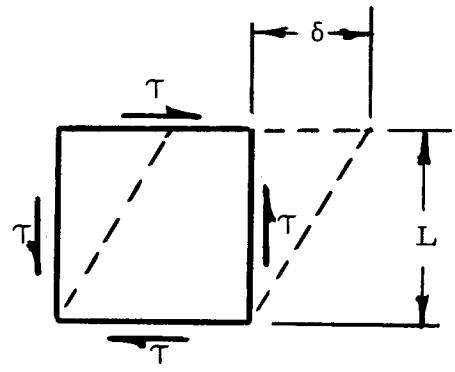

Figure 26. Shear element.

The shear strain is defined as

$$\gamma = \delta / L \tag{22}$$

and by Hooke's Law as

$$\gamma = \tau / G \tag{23}$$

where G is the shear modulus.

The work done in deforming the element is seen to be

$$W = (\tau A)(\delta)/2 \tag{24}$$

where A is the area subjected to τ.

Using Eq. (22) to rewrite Eq. (24),

$$W = (\tau A)(L\gamma)/2 \ . \tag{25}$$

And substituting Eq. (23) into Eq. (25),

$$W = (\tau A)(L\tau / G)/2 = LA(\tau^2 / 2G) \ . \tag{26}$$

Clearly, LA is the volume of the element so that the work done per unit volume is

$$w = \tau^2 / 2G \tag{27}$$

This work must equal the strain energy stored in the element per unit volume.

Now consider an element of wood subjected to the conventionally subscripted shear stresses as shown (refer to page 13 for a review of the orthotropic directions T, R, L in wood).

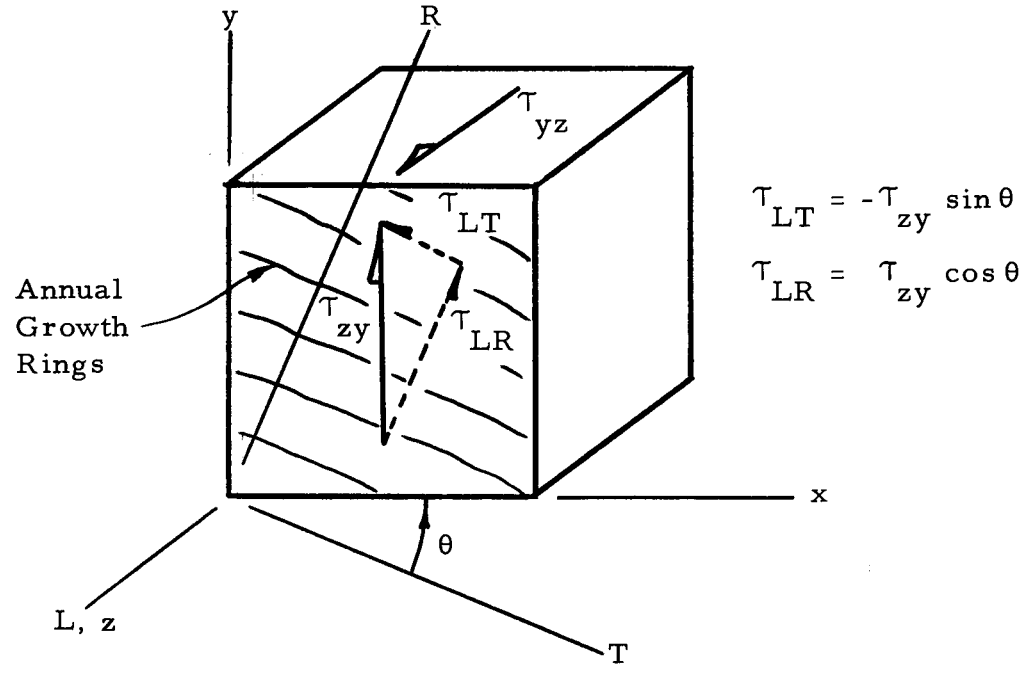

Figure 27. Element of wood in shear.

The strain energy stored in this element per unit volume by Eq. (27) is,

$$w = \tau_{zy}^2 / 2Gzy \tag{28}$$

where G_{zy} is the shear modulus for shear in the zy plane.

This strain energy must be equivalent to the strain energy associated with the stresses τ_{LT} and τ_{LR}. Thus,

$$w = \tau_{LT}^2 / 2G_{LT} + \tau_{LR}^2 / 2G_{LR} \tag{29}$$

Combining Eqs. (28) and (29),

$$\tau_{zy}^2 / 2G_{zy} = \tau_{LT}^2 / 2G_{LT} + \tau_{LR}^2 / 2G_{LR} \ . \tag{30}$$

Substituting the relations for τ_{LT} and τ_{LR} in terms of τ_{zy} from Figure 27,

$$\tau_{zy}^2 / 2G_{zy} = \tau_{zy}^2 \sin^2\theta / 2G_{LT} + \tau_{zy}^2 \cos^2\theta / 2G_{LR}$$

or

$$\frac{1}{G_{zy}} = \frac{\sin^2\theta}{G_{LT}} + \frac{\cos^2\theta}{G_{LR}} \ . \tag{31}$$

This derivation substantiates the fourth of Eqs. (7) which give the relations between elastic constants in wood under an axis rotation. To obtain the desired expression for the shear strain energy per unit volume in wood Eq. (28) is rewritten using Eq. (31),

$$w = (\tau_{zy}^2 / 2) \quad \frac{\sin^2\theta}{G_{LT}} + \frac{\cos^2\theta}{G_{LR}} \ . \tag{32}$$

Center Loaded Beam E Values

Knowing the shear strain energy in an element of wood in terms of shear stress, growth ring angle and shear moduli, it is possible to compute the shear strain energy in an entire beam under load.

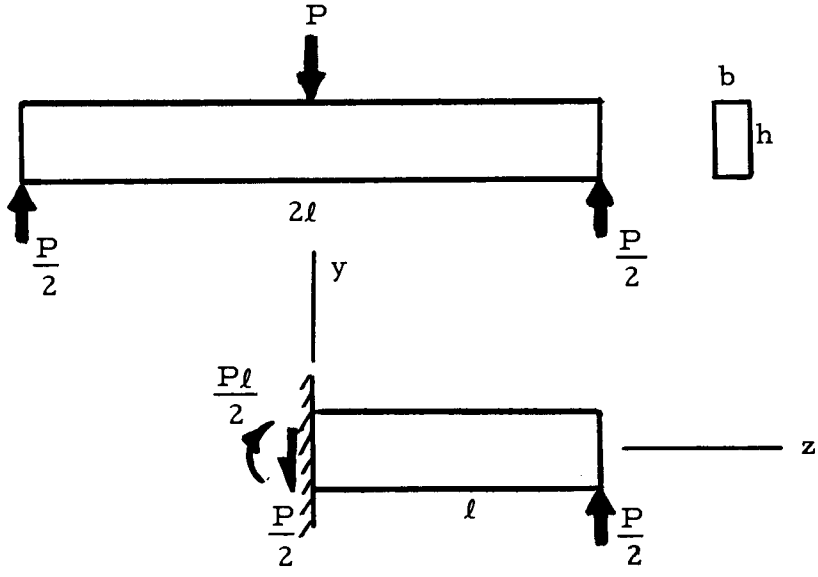

Figure 28. Simplification of a center loaded beam.

The shear strain energy in the cantilever beam shown is found by summing all the energies of the separate elements in the beam.

$$U_s = \int_{-\frac{b}{2}}^{+\frac{b}{2}} \int_{-\frac{h}{2}}^{+\frac{h}{2}} \int_{0}^{\ell} w \, dx \, dy \, dz$$

$$= \int_{-\frac{b}{2}}^{+\frac{b}{2}} \int_{-\frac{h}{2}}^{+\frac{h}{2}} \int_{0}^{\ell} \frac{\tau_{xy}^2}{2G_{zy}} \, dx \, dy \, dz \qquad (33)$$

where τ_{zy} may be a function of x, y, and z.

For the rectangular cantilever shown, the usual parabolic shear stress distribution is assumed.

$$\tau_{zy} = \frac{P}{4I_x}\left[\frac{h^2}{4} - y^2\right] \tag{34}$$

Recognizing that τ_{zy} is not a function of z or x and substituting Eq. (34) into Eq. (33),

$$U_s = \frac{b\ell}{2G_{zy}} \int_{-\frac{h}{2}}^{+\frac{h}{2}} \frac{P^2}{16I_x^2}\left[\frac{h^2}{4} - y^2\right]^2 dy$$

After integrating, the shear strain energy stored in the cantilever beam is,

$$U_s = \frac{P^2 \ell h^2}{80G_{zy} I_x} \tag{35}$$

This energy must be equivalent to the work done by the loading force $\frac{P}{2}$ in acting through the shear deflection δ_s, or

$$W = (\frac{P}{2})(\delta_s)/2 \tag{36}$$

where δ_s is the portion of the cantilever end deflection due to shear. Equating Eqs.(35) and (36),

$$\frac{P\delta_s}{4} = \frac{P^2 \ell h^2}{80 G_{zy} I_x}$$

and solving for the shear deflection,

$$\delta_s = \frac{P \ell h^2}{20 G_{zy} I_x}$$

Examination of Figure 28 shows that this is also the mid-point shear deflection of the center loaded simple beam.

The deflection due to bending is given by the common formulas for slender beams as

$$\delta_B = \frac{P \ell^3}{6EI}$$

Since shear deflection is independent of bending deflection, superposition of the two is possible.

$$\delta = \delta_s + \delta_B$$

where δ is the total deflection due to both shear and bending. Thus,

$$\delta = \frac{P \ell^3}{6EI} + \frac{P \ell h^2}{20 G_{zy} I} \tag{37}$$

$$= \frac{P \ell^3}{6EI} \left[1 + \frac{6}{20} \frac{h^2 E}{\ell^2 G_{zy}} \right]$$

Solving for E in terms of the slope $s = \delta / P$ obtained from test data,

$$E = \frac{\ell^3}{6SI}\left[1 + \left(\frac{3h^2}{10\,\ell^2}\right)\left(\frac{E}{G_{zy}}\right)\right] \tag{38}$$

Now note that from Eq. (31),

$$\frac{E}{G_{zy}} = \frac{E}{G_{LT}}\sin^2\theta + \frac{E}{G_{LR}}\cos^2\theta \tag{39}$$

The values of the ratios $\frac{E}{G_{LT}}$ and $\frac{E}{G_{LR}}$ are obtained from the Wood Handbook (47, p. 79) for Douglas Fir.

$$E/G_{LR} = 15.6$$

$$E/G_{LT} = 12.8$$

Also noting that

$$\ell = 19.5 \text{ in}$$

and substituting these values and Eq. (39) into Eq. (38),

$$E = \frac{1236}{sI}\left[1 + \frac{h^2}{1268}\left(12.8^2 + 15.5\,m^2\right)\right] \tag{40}$$

where $n = \sin\theta$

$m = \cos\theta$

Eq. (40) is used to compute E from the measured slope (s) and can be written

$$E = B/s \tag{41}$$

The factor B is computed for each specimen in Table 1 (p. 119), the slopes (s) obtained from raw data are listed in Table 3 (p. 126), and the computed values of E from Eq. (41) for the 12 specimens are listed in Table 6 (p. 123).

Third-Point Loaded Beam E Values

The third-point loaded beam is simplified as shown in Figure 29 into the two cases A and B.

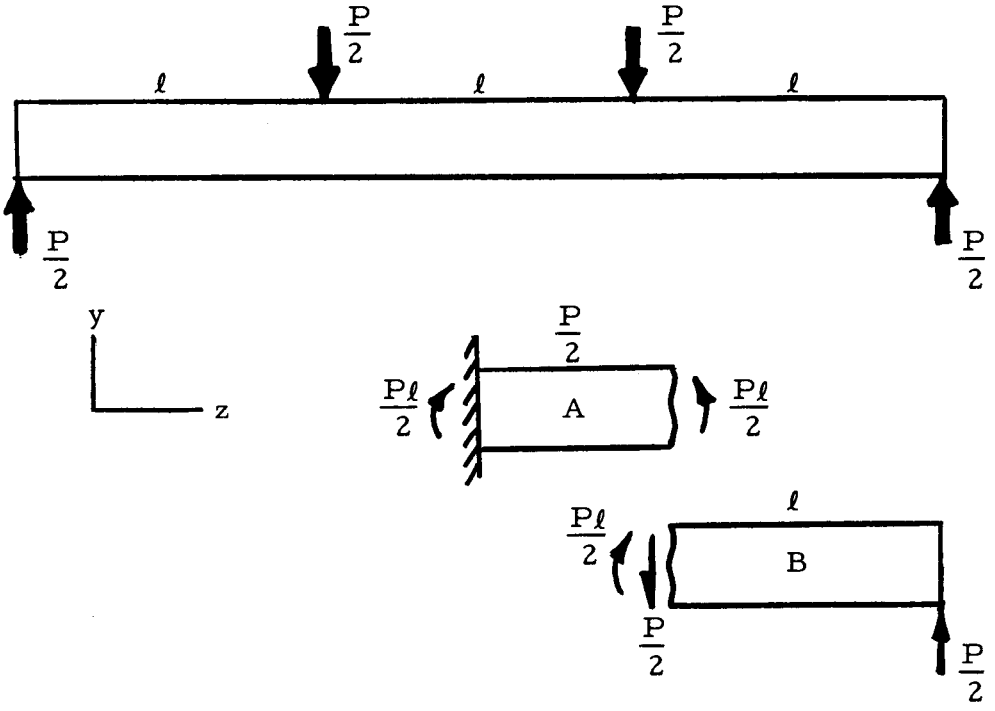

Figure 29. Simplification of a third-point loaded beam.

It is easily shown from basic beam theory that the end rotation and deflection of segment A are given by,

$$\theta_B = \frac{P\ell^2}{4EI}$$

$$\delta_A = \frac{P\ell^3}{16EI}$$

Of course, there is no shear deflection of A. Segment B is almost identical to the cantilever in Figure 28 which was shown to have the total deflection (including shear) given by Eq. (37). In addition, B undergoes a rigid rotation equal to the end rotation of A. Thus, the total end deflection of B is given by,

$$\delta_B = \frac{P\ell^3}{6EI} + \frac{P\ell h^2}{20GI} + \ell\theta_B \tag{42}$$

and the total mid-point deflection of the simple beam loaded at third-points shown in Figure 29 is,

$$\begin{aligned}\delta &= \delta_A + \delta_B \\ &= \frac{P\ell^3}{16EI} + \frac{P\ell^3}{6EI} + \frac{P\ell h^2}{20GI} + \frac{P\ell^3}{4EI} \\ &= \frac{23}{48}\frac{P\ell^3}{EI} + \frac{P\ell h^2}{20GI} \cdot \end{aligned} \tag{43}$$

Noting that $G = G_{zy}$ and that as before $s = \delta / P$, Eq. (43) can be solved for E.

$$E = \frac{\ell^3}{sI}\left[\frac{23}{48} + \left(\frac{h^2}{20\,\ell^2}\right)\left(\frac{E}{G_{zy}}\right)\right]$$

Now substituting Eq. (39) and the appropriate values for the

constants as given in the previous section, an equation similar to Eq. (40) can be written for the case of third-point loading.

$$E = \frac{1053}{sI}\left[1 + \frac{h^2}{1620}(12.8n^2 + 15.6m^2)\right] \qquad (44)$$

where $n = \sin\theta$

$m = \cos\theta$

θ is the growth ring angle as before.

Eq. (44) can be written as

$$E = D/m \, . \qquad (45)$$

The factor D is computed for each specimen in Table 1 (p. 119), the slopes (s) derived from deflection tests are listed in Table 3 (p. 120), and the values of E computed from Eq. (45) are given in Table 6 (p. 123).

It is interesting to note that the deflection due to shear represents about 11% of the total deflection for these wood beams but would represent only 2% for identical steel beams.

Strain Gage Data Reduction

Strain gage data were obtained in the form of extreme fiber strains as a function of load. For these tests it was assumed that the tension and compression properties were not identical and, therefore, the over-all or effective modulus of elasticity (E_o) was

computed on the basis that the modulus of elasticity in tension (E_t) might differ from this modulus in compression (E_c).

Figure 30 shows an assumed strain distribution and the corresponding stress distribution in the central pure bending zone of a typical test specimen.

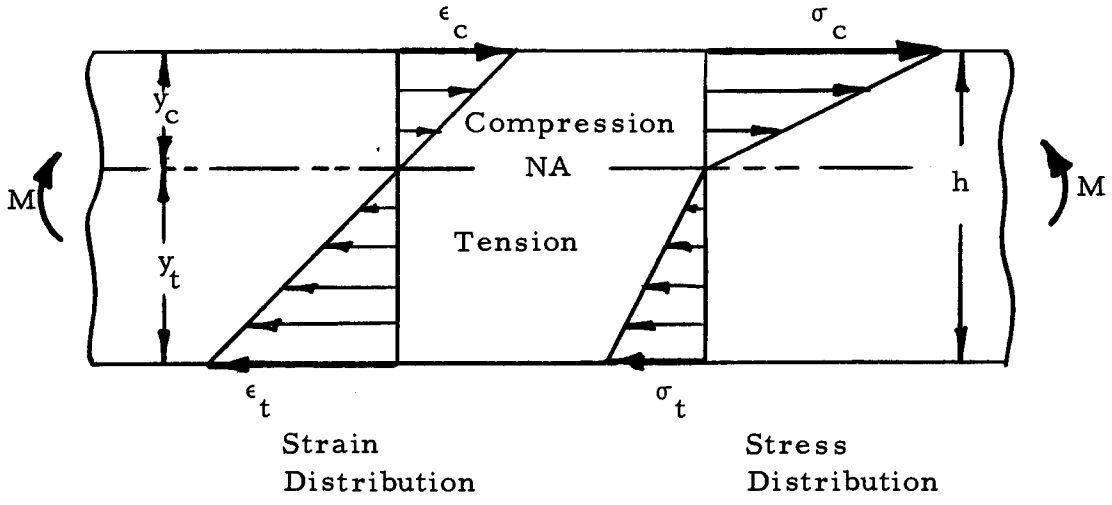

Figure 30. Stress and strain distribution in pure bending section of wood beam.

The assumptions made are that the beam is homogeneous along its longitudinal axis and that the modulus of elasticity is constant though perhaps different in tension and compression. The first assumption provides that plane sections must remain plane and that the strain varies linearly from top to bottom as shown. The second assumption provides that the stress in the beam must be a linear function of the distance from the neutral axis but that this function is not necessarily

the same above and below the axis as shown in Figure 30. The following definitions for the different moduli can be made from Figure 30.

$$E_L = \frac{\sigma_c}{\epsilon_L}, \quad E_t = \frac{\sigma_t}{\epsilon_t} \tag{46}$$

$$E_o = \frac{y_c}{h} E_c + \frac{y_t}{h} E_t \tag{47}$$

where σ_c, σ_t are the maximum fiber stresses in compression and tension.

ϵ_L, ϵ_t are maximum fiber strains in compression and tension.

$\frac{y_c}{h}$, $\frac{y_t}{h}$ are the fractions of the beam exposed to compression and tension.

Representative values for ϵ_c and ϵ_t at a particular load can be determined from strain gage data and the values of σ_c and σ_t are then fixed by equilibrium considerations.

Maximum Fiber Strains from Strain Gage Data

The readings from each gage were plotted against load; very linear curves were obtained for both tension and compression gages. A straight line was drawn through the plotted points for each gage and the value of strain at the arbitrary load of P = 1500 lb. was recorded from this line. For each pair of gages located on the same

face of a specimen, the recorded strains were averaged. These averages represent the most accurate maximum fiber strains at P = 1500 obtainable from the data and were used as ϵ_c and ϵ_t in Eqs. (46).

Maximum Fiber Stresses from Equilibrium

The moment in a beam in terms of the longitudinal stress is found from equilibrium considerations,

$$M = \int_A \sigma\, y\, dA$$

where A is the cross-sectional area.

y is the variable distance from the neutral axis to the element dA.

σ is the normal stress acting on element dA.

This integral can be evaluated by inspection of the stress distribution in Figure 30.

$$M = \left[\frac{\sigma_c y_c b}{2}\right] \frac{2}{3} y_c + \left[\frac{\sigma_t y_t b}{2}\right] \frac{2}{3} y_t \qquad (48)$$

where b is the beam's thickness.

The factors in brackets represent the total compressive and tensile forces acting at the centroids of their respective regions and the remaining factors are the moment arms from the neutral axis to the

centroids. In order that force equilibrium be satisfied the bracketed factors must also be equivalent.

$$\frac{\sigma_c y_c b}{2} = \frac{\sigma_t y_t b}{2}$$

or,

$$\sigma_c y_c = \sigma_t y_t \tag{49}$$

The following formulas for the location of the neutral axis can be derived from the similar triangles of the strain distribution in Figure 30.

$$y_t = \frac{\epsilon_t h}{\epsilon_t + \epsilon_c}$$

$$y_c = \frac{\epsilon_c h}{\epsilon_t + \epsilon_c} \tag{50}$$

Eqs. (48), (49), and (50) can be solved for the desired maximum fiber stresses σ_c and σ_t.

Equations for E Values

From Eqs. (46),

$$\sigma_c = E_c \epsilon_c$$

$$\sigma_t = E_t \epsilon_t \ . \tag{51}$$

Substituting these and Eqs. (50) into Eq. (49),

$$\epsilon_t^2 E_t = \epsilon_c^2 E_c \quad . \tag{52}$$

Eq. (48) can be rewritten,

$$\sigma_c y_c^2 + \sigma_t y_t^2 = \frac{3M}{b} \quad . \tag{53}$$

Substituting Eqs. (50) and (51) into the left side of Eq. (53),

$$E_t \epsilon_t^3 + E_c \epsilon_c^3 = \frac{3M(\epsilon_t + \epsilon_c)^2}{bh^2} \quad . \tag{54}$$

Now using Eq. (52) in Eq. (54),

$$\epsilon_c^2 E_c \epsilon_t + E_c \epsilon_c^3 = \frac{3M(\epsilon_t + \epsilon_c)^2}{bh^2} \quad .$$

Solving for E_c

$$E_c = \frac{3M}{bh^2} \left[\frac{\epsilon_t + \epsilon_c}{\epsilon_c^2} \right] \tag{55}$$

similarly,

$$E_t = \frac{3M}{bh^2} \left[\frac{\epsilon_t + \epsilon_c}{\epsilon_t^2} \right] \quad . \tag{56}$$

By substituting Eqs. (50), (55), and (56) into Eq. (47) and simplifying,

$$E_o = \frac{3M}{bh^2} \left[\frac{\epsilon_t + \epsilon_c}{\epsilon_t \epsilon_c} \right] \quad . \tag{57}$$

Since the maximum fiber strains were obtained at P = 1500 lb., the corresponding moment M from Figure 29 is seen to be ,

$$M = \frac{P\ell}{2} = \frac{(1500)(13)}{2} = 9750 \text{ in-lb.}$$

The common factor $(\frac{3M}{bh^2})$ with M = 9750 in-lb. is computed for each specimen in Table 1 (p. 119). The values of all strain gage readings corrected to P = 1500 lb. as well as the values of ϵ_c and ϵ_t are given in column (5) of Table 4 (p. 121). (Recall for this table that ϵ_c is the average of strains measured by gages 1 and 2 and ϵ_t is the average of gages 3 and 4.) The final values of E_o computed from Eq. (57) are given in Table 6 (p. 123).

Photoelastic Data Reduction

Part of the photoelastic data was obtained in the form of fringe pattern photographs. A composite of these is shown in Figure 31. The fringe pattern for each specimen is composed of the left half of the whole-order fringe photograph and the right half of the half-order fringe photograph. The zero-order fringe is marked for each specimen along the vertical centerline of each fringe pattern. For the analysis, a tracing was made of each data photograph superimposing the two fringe orders for each specimen. These tracings are shown in Figure 41 (p. 117). Examination of Figure 31 shows that the location of the zero-order fringe for some of the fringe

patterns is not where the neutral axis of the beam would be expected. As mentioned earlier (p. 62) this was found to be caused by a uniform residual strain in the coating which has the effect of introducing a constant error to all strain readings taken from the photoelastic data. To correct for this constant error, new tests were made and special attention was given to subtracting out the residual strains by adjustment of the polariscope. The objective of the new tests was to determine the position of the true neutral axis in each specimen. The exact method of using this new information to correct the existing data is given in a later section. The positions of the neutral axes measured from the bottom of each beam as determined from the new tests are given in column (1) of Table 5 (p. 122).

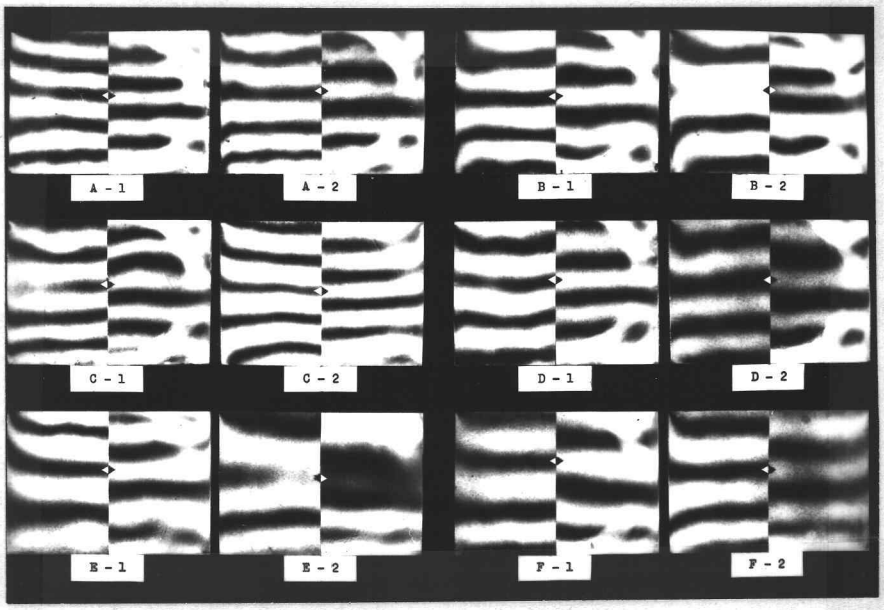

Figure 31. Composite of photoelastic data photographs.

Correction Factors for Reinforcing Effects

Stieda (40, p. 356) shows that the following equations developed by Zandman (53) apply to wood when the principal stresses lie along orthotropic axes.

$$(\epsilon_z - \epsilon_y)_{actual} = \frac{(\epsilon_z - \epsilon_y)_{observed}}{C} \tag{58}$$

with

$$C = \left[1 + \frac{t_c E_c}{t_s E_s} \frac{(1 + \nu_s)}{(1 + \nu_c)}\right]^{-1} \tag{59}$$

where s implies structure.

c implies coating.

t, E, ν are thickness, modulus of elasticity and Poisson's ratio.

The approximate values of E_s and ν_s are taken from the Wood Handbook (47, p. 75-79) but since the value of ν_s will vary with growth ring orientation, the factor C will also vary for each test beam. The variance was negligible, however, and the value of C for all specimens is 0.988.

Relation of Fringes to Longitudinal Strains

The coating used has a fringe value (f) of 940 μin/in/fringe so that the observed principal strain difference is given by,

$$(\epsilon_z - \epsilon_y)_{observed} = 940\, n \tag{60}$$

where n_f is the fringe number and is not necessarily an integer since fractional fringe orders are obtained by a rotation of the analyzer.

The actual principal strain difference can be defined by consideration of Figure 32.

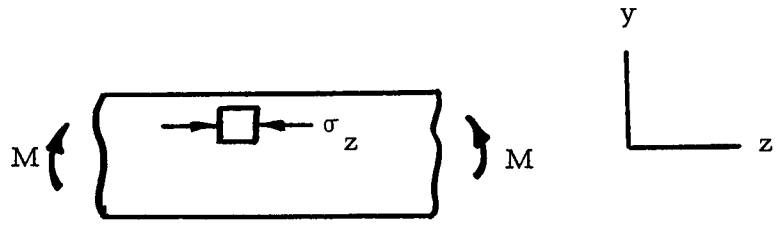

Figure 32. Typical element in pure bending section of test beam.

From Hooke's Law for the typical element shown,

$$\sigma_z = E\,\epsilon_z$$

$$\epsilon_y = -\frac{\nu}{E}\,\sigma_z = -\nu\epsilon_z \quad .$$

Thus,

$$(\epsilon_z - \epsilon_y)_{actual} = (1 - \nu)\epsilon_z \quad . \tag{61}$$

Now combining Eqs. (58), (60), and (61) and solving for ϵ_z / n_f

$$\frac{\epsilon_z}{n_f} = \frac{940}{C\,(1+\nu)} \quad . \tag{62}$$

To make this relation useful in reducing test data, the value of ν must be determined. It is understood that ν is the Poisson's ratio of contraction in the y direction to elongation in the z direction and, therefore, can be subscripted ν_{zy}. Figure 33 shows a typical specimen and illustrates the need to relate ν_{zy} to the known properties ν_{LR} and ν_{LT}.

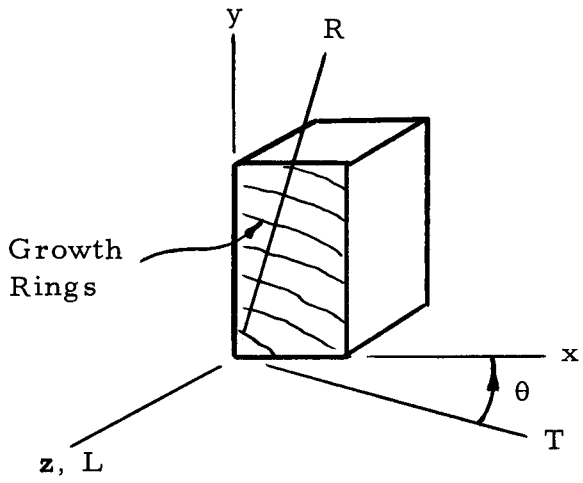

Figure 33. Growth ring orientation in typical test specimen.

The ninth of Eqs. (7) (p. 18) gives the needed relation which can be written

$$\nu_{zy} = \nu_{LT} n^2 + \nu_{LR} m^2 \qquad (63)$$

where $n = \sin\theta$

$m = \cos\theta$.

From the Wood Handbook (47, p. 79) for Douglas Fir,

$$\nu_{LR} = .292$$

$$\nu_{LT} = .449 \ .$$

The values of n^2 and m^2 are listed in Table 1 (p. 119) and ν_{zy} is listed for each specimen in Table 5 (p. 122).

The factor ϵ_z/n_f given by Eq. (62) is computed for each specimen in column (5) of Table 5 (p. 122).

Determination of E Values

The modulus of elasticity was computed from photoelastic data in the following manner.

1. Vertical centerlines were drawn on the fringe photograph tracings as shown in Figure 41 (p.117).
2. The distance measured from the beam's bottom edge to the point where each fringe intersects the vertical centerline was recorded in Table 5 (p. 122).
3. Each fringe was labeled for its order (n) and the factor computed from Eq. (62) was used to convert these fringe values to longitudinal strain values (ϵ_z) which are given in Table 5 (p. 122).
4. The information from steps 2 and 3 was plotted and a straight line fitted to obtain a strain distribution for each

beam as shown in Figure 34.

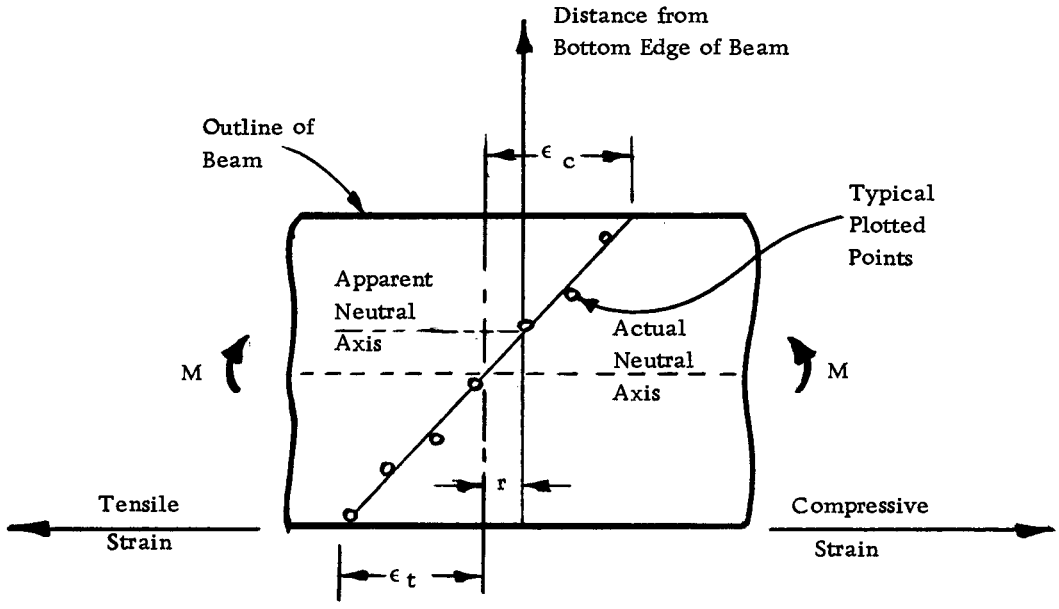

Figure 34. Example strain distribution from photoelastic data.

5. The location of the actual neutral axis given for each beam in column (1) of Table 5 (p. 122) was used to position the neutral axis on the strain distribution as shown in Figure 34.

6. The residual strain (r) that was found to be in the coatings was determined as shown in Figure 34 and the actual corrected maximum fiber strains ϵ_t and ϵ_c were then fixed as shown. These strains are recorded for each specimen in columns (2) and (3) of Table 5 (p. 122).

7. The values of ϵ_t and ϵ_c were used in Eq. (57) to compute the effective modulus of elasticity E_o in the same way that the values of ϵ_t and ϵ_c determined from strain gage data

were used. The values of E_o are given for each specimen in Table 6 (p. 123).

Statistical Analysis

To appraise the photoelastic coating technique, a statistical analysis is required. The two flexure tests (midpoint and third-point loading) are assumed to be the standard for providing "true" values of the elastic moduli of the 12 specimens. A measure of the accuracy of the elastic moduli obtained from the photoelastic technique can then be determined.

The relationship between two variables can be studied by regression analysis, i.e., curve fitting. By plotting corresponding values of the variables as abscissas and ordinates, a curve may be fitted by the method of least squares. An equation related the variables can then be derived. Consider the midpoint loading test results (M) i.e., the "true" values, as one variable and the photoelastic test results (P) as the other. A linear curve can be fitted to the 12 sets of test results by the method of least squares. The curve is expressed by Eq. (1):

$$M = a + bP \tag{1}$$

This equation predicts the "true" value (M) for a given value of P. The accuracy of the predicted values can be determined from

confidence curves representing upper and lower limits within which a given percentage of data will fall. Typical confidence curves are shown in Fig. 35.

The fitted curve will always pass through the grand mean, a point whose coordinates are the means of the two variables. Also at the grand mean the confidence curves reach a minimum separation. In the neighborhood of this point the confidence curves can be expressed as

$$M = a + bP \pm t\sigma \qquad (2)$$

Where σ is the standard deviation of the measured and predicted values of M and t is the Student's statistic for the desired confidence level.

Since the values of P (the measured elastic moduli for the 12 boards) do not vary much, but rather are grouped around their mean, the confidence curves for the entire range of P are approximated by Eq. (2). This equation expresses the expected deviation of the photoelastic data, P, from the "true" or standard data, M, for a chosen confidence level.

The regression procedure was also used to compare the other test methods. The variation of the elastic moduli from the standard value in psi, and as a percentage of the standard mean is given in Table 7 (p. 124) for the 90% and 95% confidence levels.

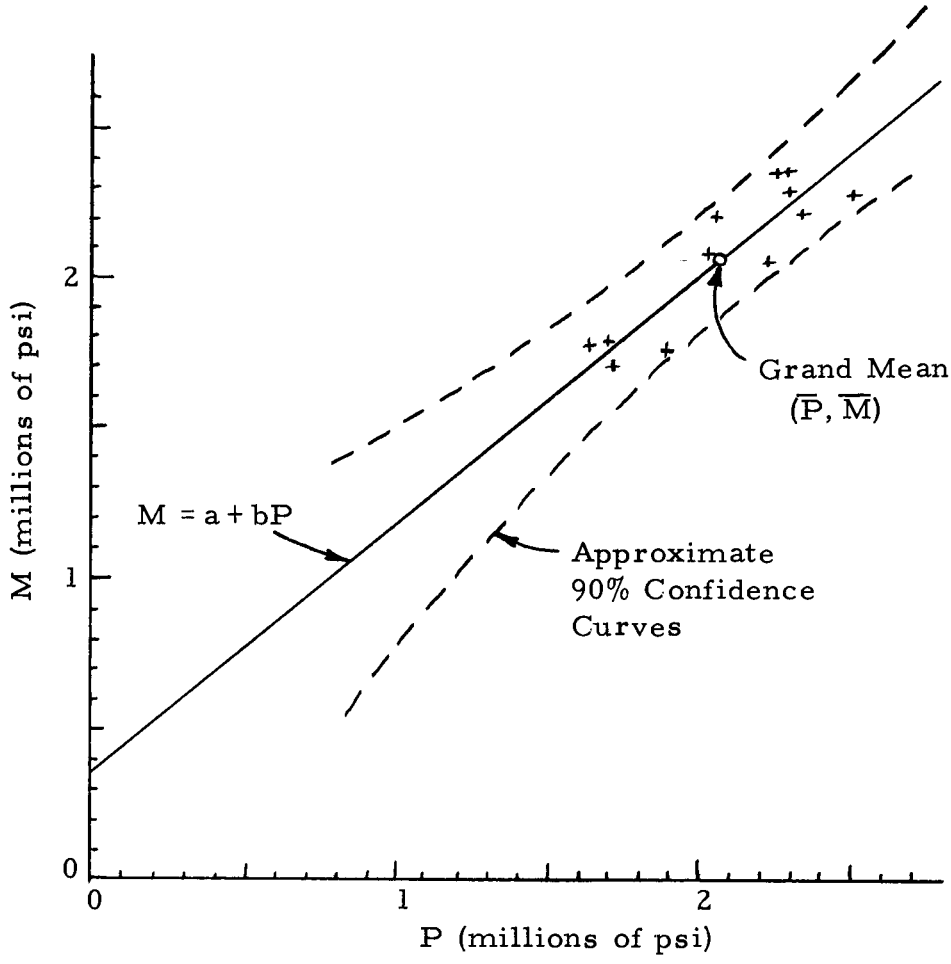

Figure 35. Typical Confidence Curves for M.

Laminated Beam Data Reduction

The photographs obtained showing the strain patterns around butt joints required no reduction for the qualitative analysis that was made. For convenience, however, the photographs were traced on vellum and the analysis was made on the tracings. A composite of the photographs is shown in Figure 36 and the tracing of this is shown in Figure 42 (p. 118).

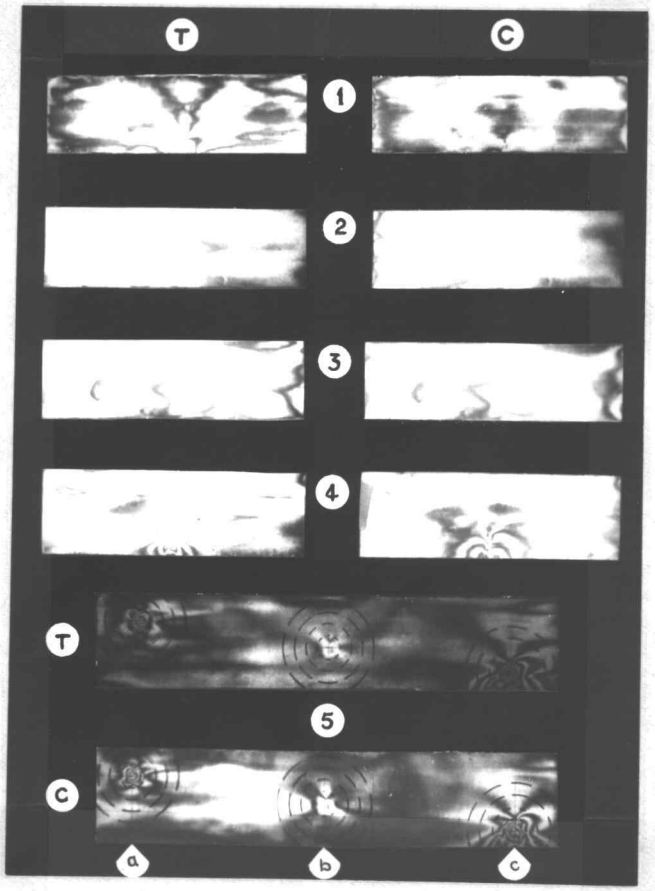

T indicates longitudinal tension.
C indicates longitudinal compression.

Figure 36. Composite of Laminated Beam Data.

VII. RESULTS

Comparative Tests

Values for the modulus of elasticity determined for each beam from the four test methods are compared in Figure 37 (p. 113). The deviation of the elastic moduli from the standard for each test method is given in Table 7 (p. 124). A comparison of strain distributions for the strain gage and photoelastic tests is shown in Figures 38, 39, and 40.

Laminated Beam Tests

Tracings of the butt joint fringe photographs appear in Figure 42 (p. 118). These tracings show the outline of photoelastic fringes which indicate the nature of the stress distribution near a butt joint.

VIII. CONCLUSIONS AND RECOMMENDATIONS

Comparative Tests

Accuracy of the Photoelastic Method on Wood

The statistical analysis shows that the photoelastic coating method on wood can be trusted within about 10% in nine out of ten tests and within about 13% in 19 out of 20 tests. It must be emphasized that these inferences are based on very specific tests and test methods. Extensions of the inferences to other problem types should be made with caution.

Note that this estimated error is conservative. It is actually a statement of how closely the photoelastic measurements agree with the standard deflection test measurements. Assuming the latter to be exact, the photoelastic measurements contain all of the error in both tests. The close correlation between the two deflection test methods, however, indicates that the error in these tests is small.

Sources of Error. It is important to recognize the factors that contribute to the error in the photoelastic method. With proper effort these factors may be eliminated, reduced or compensated for in future applications.

Probably the most apparent factor is the error occurring in reduction of photographic data. As shown in Figure 30 (p. 82),

the fringes recorded cannot be precisely measured because of their width and lack of distinctness. This factor could be reduced by sharpening the fringes or by increasing their number. Since increasing the number of fringes requires thicker coatings or higher loads for a given plastic, fringe sharpening appears to be the most suitable.

Another factor causing error is the estimate of Poisson's ratio for the wood being tested. To reduce the raw photoelastic data the average value of Poisson's ratio for the species was used instead of the actual value for each individual specimen. Since it has been found (24, p. 5) that the values of Poisson's ratio will fluctuate at most ±33% from the average for the Douglas Fir species, it is likely that error is introduced by using average values. From the equations used in data reduction it can be shown that an extreme deviation (33%) from the species average will cause about 8% error in the final result. How often extreme deviations occur is not known. But some information about this type of error can be found in Figure 37 (p. 113). Certainly the end-matched specimens A-1 and A-2 should have almost the same Poisson's ratio and therefore should have about the same error caused by incorrectly estimating Poisson's ratios. A comparison shows, however, that the errors are quite different. This indicates that the error due to inexact Poisson's ratios is a minor part of the total error.

Another possible factor of error has to do with changes in the specimens caused by repeated loading. A change in the modulus of elasticity of the specimens brought on by the repeated loading would invalidate comparisons between the tests. This factor is thought to be negligible because of tests made by the U. S. Forest Products Laboratory (51, p. 21). These show that while considerable creep occurs, the modulus of elasticity remains constant when Douglas Fir is loaded repeatedly.

Limitations and Technical Problems

Probably the most serious limitation of the photoelastic coating method applied to wood is caused by the reinforcing effect of the coating. This effect is easily compensated for in simple situations. But for complex strain distributions the correction factors for reinforcing effects are variables. The difficulty is especially noticeable when considering strain distributions around natural imperfections such as knots. In these areas the photoelastic coating tends to distribute the stresses and thus reduce the effects due to any stress concentrations.

Another problem arises when the coating method is applied to wood. Permanent or residual strains appear in the coating after it is cemented to the surface. One reason for these strains is thought to be a reaction between wood and cement. As the cement is applied

some of it penetrates into the surface of the wood. This causes a reaction between the wood and the cement affecting the coating. A thin layer of cement applied and allowed to set prior to the placement of the photoelastic coating solves this problem.

Another reason for residual strains are changes in temperature and humidity. A gain or loss of moisture to the air or a change of temperature causes expansion or shrinkage of the coated wood. This in turn creates residual strain patterns on the coating. This effect may be minimized by completing the tests as soon as possible after the specimens are prepared or by keeping them in a controlled environment.

A technical problem of a different kind is the complexity of specimen preparation and data reduction required for the photoelastic technique. Considerable skill and knowledge is required by the operator both during the testing and data reduction phase.

Recommendations

It has been noted that the accuracy of the photoelastic method applied to wood could be improved by sharpening and multiplying fringes without increasing coating thickness. Work has been done in this area by a number of investigators (2, 7, 9, 14, 32) using optical and photographic techniques.

The most serious difficulty with the coating method and all

other methods is the complex nature of the wood itself. A prerequisite for successful stress analysis is some understanding of the mechanical behavior of wood. A thorough review of recent literature on this subject was done by Youngs (52). He lists 356 references.

Laminated Beam Test Conclusions

The objective of the laminated beam tests is to answer certain questions about the effects of butt joints. These questions and their answers are discussed in the following section.

First, at what distance must butt joints be separated to eliminate the interaction of their individual stress concentrations? Looking at Figure 41 (p. 117) and considering cases of butt joints in interior laminae one can note that the outlines of higher strain levels extend no more than a distance equal to six laminae thicknesses from the joint. It is inferred from this that a butt joint separation of a distance equal to 12 laminae thicknesses is sufficient to eliminate the interaction of their individual stress concentrations. This applies to butt joints in interior laminae and is independent of the relative position of the laminae, eg. the joints may be in the same laminae, adjacent laminae, or in laminae separated by one or more other laminae.

Now consider the effects of butt joints in exterior laminae.

From the single example of specimen number one in Figure 41 (p. 117), the safe separation from any interior butt joint appears to be a distance equal to 16 laminae thicknesses.

Recall that the strain patterns outlined in Figure 41 were made from beams stressed to the maximum working stress of 3020 psi. Higher stresses will require a larger joint separation to avoid interaction.

Second, to what extent does the size of the gap at a butt joint effect the stress concentration caused by that joint? An examination of the strain pattern tracings of specimens #2, #3, and #4 will help answer this. Butt joint #2 has twice the gap of butt joint #3 but there is very little difference between their stress concentrations. On the other hand butt joint #4 has no gap but has a stress concentration twice that of either #2 or #3. All this indicates that gap size is probably insignificant when comparing large gaps with other large gaps but that very small gaps have significantly higher stress concentrations than large gaps.

Third, to what extent does a well glued butt joint reduce the stress concentration? Strain pattern tracings of the specimens #1, #4, and #5b show strain patterns for glued butt joints. In the case of #1 and #4 concentration reduction is found in compression but not in tension. The glue has apparently acted as a filler, supporting in compression but failing in tension. The case of #5b on the other

hand shows a marked stress concentration reduction in both compression and tension. Evidently the joint has been mated and glued well enough to withstand the applied tensile stress. The conclusion is this: glued butt joints have a distinct advantage in compression. In tension the advantage depends on the integrity of the glue bond.

Fourth, is there any significant difference between the stress concentration caused by a butt joint in tension and a butt joint in compression? Aside from the difference pointed out in the previous discussion about glued joints, the strain pattern tracings indicate no difference.

Fifth, what is the approximate magnitude of the stress concentration caused by a butt joint? Look at the example of a six ply laminated beam such as those tested. They have been loaded to a stress, say σ . Elementary formulas predict a maximum stress equal to $6/5 \cdot \sigma$ at a cross section having a butt joint in one of the laminae. Of course in reality the maximum stress will be larger due to the stress concentration effect. Now define the stress concentration factor (K) as the ratio of the actual maximum induced stress to the stress computed by the elementary formula. It should be possible to get a rough estimate of K from the strain pattern tracings in Figure 41 (p. 117). The test beams have been stressed to about 3000 psi or approximately two fringes of strain. The

elementary formula predicts 6/5 ths of this or about 2.4 fringes. A count of the number of fringes in the tracings shows an actual maximum strain of from 5 to 7 fringes. The value of K is thus about 2 or 3. This is at best a rough estimate because of the way that the photoelastic coating covers the butt joint and reinforces it. The coating must conform exactly to the contour of the surface if an accurate estimate is to be made.

There is another approach to finding K more accurately. Transparent photoelastic models of a laminated structure could be made for use in a transmission polariscope.

A more detailed investigation of the stress distribution around butt joints in laminated lumber is presently under investigation at Oregon State University and will be reported on in a later thesis.

BIBLIOGRAPHY

1. Asano, I. and K. Tsuzuki. Studies of strain measurement in wood by electrical resistance wire strain gage. Journal of the Japan Wood Research Society 6 (4):140-4. 1960.

2. Bynum, Douglas, Jr. On the accuracy of fringe multiplication with mirrored birefringent coatings. Experimental Mechanics 6(7):381-386. 1966.

3. Cheng, Y. F. Some experimental techniques for employing a continuous-wave gas laser as a light source in scattered-light static photoelasticity. Experimental Mechanics 6(8):431-437. 1966.

4. Coker, E. G. and L. N. G. Filon. A treatise on photoelasticity. London, Cambridge University Press, 1930. 418 p.

5. Cunningham, J. H. and J. M. Yavorsky. The brittle lacquer technique of stress analysis as applied to anisotropic materials. Proceedings of the Society for Experimental Stress Analysis 14(2):101-107. 1957.

6. Dahlke, H. J. Photoelastic methods in the stress analysis of wood. Corvallis, Oregon. June 15, 1965. 8 numb. leaves. (Weyerhaeuser Company Technical Center, Longview, Washington. Appendix A to report no. RDR)

7. Dally, J. W. and F. J. Ahimaz. Photographic method to sharpen and double isochromatic fringes. Experimental Mechanics 2(6):170-181. 1962.

8. Dally, J. W. and W. F. Riley. Experimental stress analysis. New York, McGraw-Hill, 1965. 498 p.

9. Day, E. E., A. S. Kobayashi and C. N. Larson. Fringe multiplication and thickness effects in birefringent coatings. Experimental Mechanics 2(4):115-121. 1962.

10. Dove, R. C. and Paul H. Adams. Experimental stress analysis and motion measurement. Columbus, Ohio, Charles E. Merrill, 1964. 515 p.

11. Drucker, D. C. Photoelastic separation of principal stresses by oblique incidence. Journal of Applied Mechanics 10(3): A156-A160. 1943.

12. Duffy, J. Effects of thickness of birefringent coatings. Experimental Mechanics 1(3): 74-82. 1961.

13. Durelli, A. J. and W. F. Riley. Introduction to photomechanics. Englewood Cliffs, N. J., Prentice-Hall, 1965. 402 p.

14. Flanagan, J. H. Photoelastic photography. Proceedings of the Society for Experimental Stress Analysis 15(2): 1-14. 1958.

15. Frocht, M. M. Photoelasticity. New York, John Wiley and Sons, 1941. 2 vols.

16. Hatayama, Y. Mechanical properties analysis of wood by means of brittle lacquer. Journal of the Faculty of Agriculture, Iwate University 4(4): 380-387. 1960.

17. Hearmon, R. F. S. Applied anisotropic elasticity. London, Oxford University Press, 1961. 153 p.

18. _____. Elasticity of wood and plywood. London, 1950. 87 numb. leaves. (Great Britian. Department of Scientific and Industrial Research. Forest Products Research Board. Special report no. 7)

19. _____. Theory of elasticity of orthotropic materials. In: Proceedings of the Conference on the Mechanical Behavior of Wood, University of California, Berkeley, 1962. Berkeley, University of California, 1963. p. 84-95.

20. Hendry, A. W. An introduction to photoelastic analysis. Glasgow, Blackie and Son, 1948. 463 p.

21. Hetenyi, M. I. (ed.) Handbook of experimental stress analysis. New York, John Wiley and Sons, 1950. 1077 p.

22. Ickovic, E. A. The direction of the stresses in wood when a cutter penetrates it. Izvestiia Vysshikh Uchebnyka Zavedenii. Lesnoi Zhurnal, Archangel, Russia 6(3): 114-118. 1963.

23. Lekhnitskii, S. G. Theory of elasticity of an anisotropic elastic body. Tr. by P. Fern. San Francisco, Holden-Day, 1963. 404 p.

24. McBurney, R. S. and J. T. Drow. The elastic properties of wood. Young's moduli and Poisson's ratios of douglas fir and their relations to moisture content. Madison, Wis., 1946. 8 numb. leaves. (U. S. Forest Products Laboratory report no. 1528-D. Reaffirmed 1962)

25. Maku, T. and H. Sasaki. Strain determination of wood by coating. Journal of the Japan Wood Research Society 6(2): 58-70. 1960.

26. _____. Stress analysis of wood by brittle coating. Translations of the Commonwealth Scientific Industrial Research Organization, Australia, no. 6435: 1-23. 1963. (Translated by M. Fremt from Holz Roh-und Werkstoff 20(8): 303-314. 1962) (Abstracted in Forestry Abstracts 25(4): no. 5639. 1964)

27. March, H. W. Stress stain relations in wood and plywood considered as orthotropic materials. Madison, Wis., 1944. 24 numb. leaves. (U. S. Forest Products Laboratory report no. 1503)

28. Morris, W. H. M. and I. Jansson. A photoelastic method for studying the stresses in wood. Lafayette, Indiana, 1957. n. p. (Purdue University report. Weyerhaeuser Technical Center Library)

29. Norris, C. B. The application of Mohr's stress and strain circle to wood and plywood. Madison, Wis., 1943. 19 numb. leaves. (U. S. Forest Products Laboratory report no. 1317)

30. _____. Strength of orthotropic materials subjected to combined stresses. Madison, Wis., 1950. 19 numb. leaves. (U. S. Forest Products Laboratory report no. 1816)

31. North, W. P. T. and C. E. Taylor. Dynamic-stress concentration using photoelasticity and a laser light source. Experimental Mechanics 6(7): 337-343. 1966.

32. Post, D. Isochromatic fringe sharpening and fringe multiplication in photoelasticity. Proceedings of the Society for Experimental Stress Analysis 12(2): 143-156. 1955.

33. Post, D. and F. Zandman. Accuracy of the birefringent-coating method for coatings of arbitrary thickness. Experimental Mechanics 1(1):21-32. 1961.

34. Radcliffe, B. M. A method for determining the elastic constants of wood by means of electric resistance strain gages. Forest Products Journal 5(1):77-84. 1955.

35. Schniewind, A. P. Mechanism of check formation. Forest Products Journal 13(11):475-480. 1963.

36. Sliker, A. Electrical resistance strain gages, their zero shift when bonded to wood. Forest Products Journal 9(1):33-38. 1959.

37. Slot, Thomas. Reflection polariscope for photography of photoelastic coatings. Experimental Mechanics 2(2):41-47. 1962.

38. Smith, C. B. and A. W. Voss. Stress distribution in a beam of orthotropic material subjected to a concentrated load. Washington, D. C., 1948. 39 numb. leaves. (U. S. National Advisory Committee for Aeronautics. Technical note no. 1486)

39. Sokolnikoff, I. S. Mathematical theory of elasticity. New York, McGraw-Hill, 1956. 476 p.

40. Stieda, C. K. A. Photostress analysis of timber structures. In: Proceedings of Second Symposium on the Non-destructive Testing of Wood, Spokane, Washington, 1965. Pullman, Washington, Washington State University, 1965. p. 349-370.

41. _____. Stress concentrations in notched timber beams. Transactions of the Engineering Institute of Canada 7(10):A5-A11. 1964.

42. Takahashi, A. Strain determination on wood by using photoelastic coating technique, IV. The strain distributions of the cross section (Pog) under diametral compression. Journal of the Japan Wood Research Society 11(1):7-13. 1965.

43. Takahashi, A. and K. Nakato. Strain determination on wood by using the photoelastic coating technique, I and II. On the photoelastic character of modified epoxy resin. Journal of the Japan Wood Research Society 10(2):49-61. 1964.

44. _____. Strain determination of wood by using photoelastic coating technique, III. On the relation between elastic modulus and the strain distributions of photoelastic coating. Journal of the Japan Wood Research Society 10(5):176-181. 1964.

45. Taylor, C. E. et al. Applications of lasers to photoelasticity. Experimental Mechanics 6(6):289-295. 1966.

46. Theocaris, P. S. and K. Dafermos. A critical review on the thickness effects of birefringent coatings. Experimental Mechanics 4(9):271-276. 1964.

47. U. S. Forest Products Laboratory. Wood handbook. Washington, D. C., 1955. 528 p. (U. S. Dept. of Agriculture. Agriculture Handbook no. 72)

48. Voigt, W. Lehrbuch der Krystallphysik. Leipzig, Germany, Teubner, 1910. n. p.

49. Walker, J. N. Interpretation and measurement of strains in wood. (Abstract) Dissertation Abstracts 22(1):189-190. 1961.

50. Yavorsky, J. M. and J. H. Cunningham. Strain distribution in maple glue block shear specimen as indicated by a brittle lacquer. Forest Products Journal 5(1):80-86. 1965.

51. Youngquist, W. G. Performance of bonded wire strain gages on wood. Madison, Wis., 1957. 26 numb. leaves. (U. S. Forest Products Laboratory report no. 2087)

52. Youngs, R. L. Recent progress towards an understanding of the physical and mechanical properties of wood. Forest Products Journal 11(5):215-225. 1961.

53. Zandman, F., S. S. Redner and E. I. Riegner. Reinforcing effect of birefringent coatings. Experimental Mechanics 2(2):55-64. 1962.

APPENDICES

APPENDIX A

MISCELLANEOUS TABLES AND FIGURES

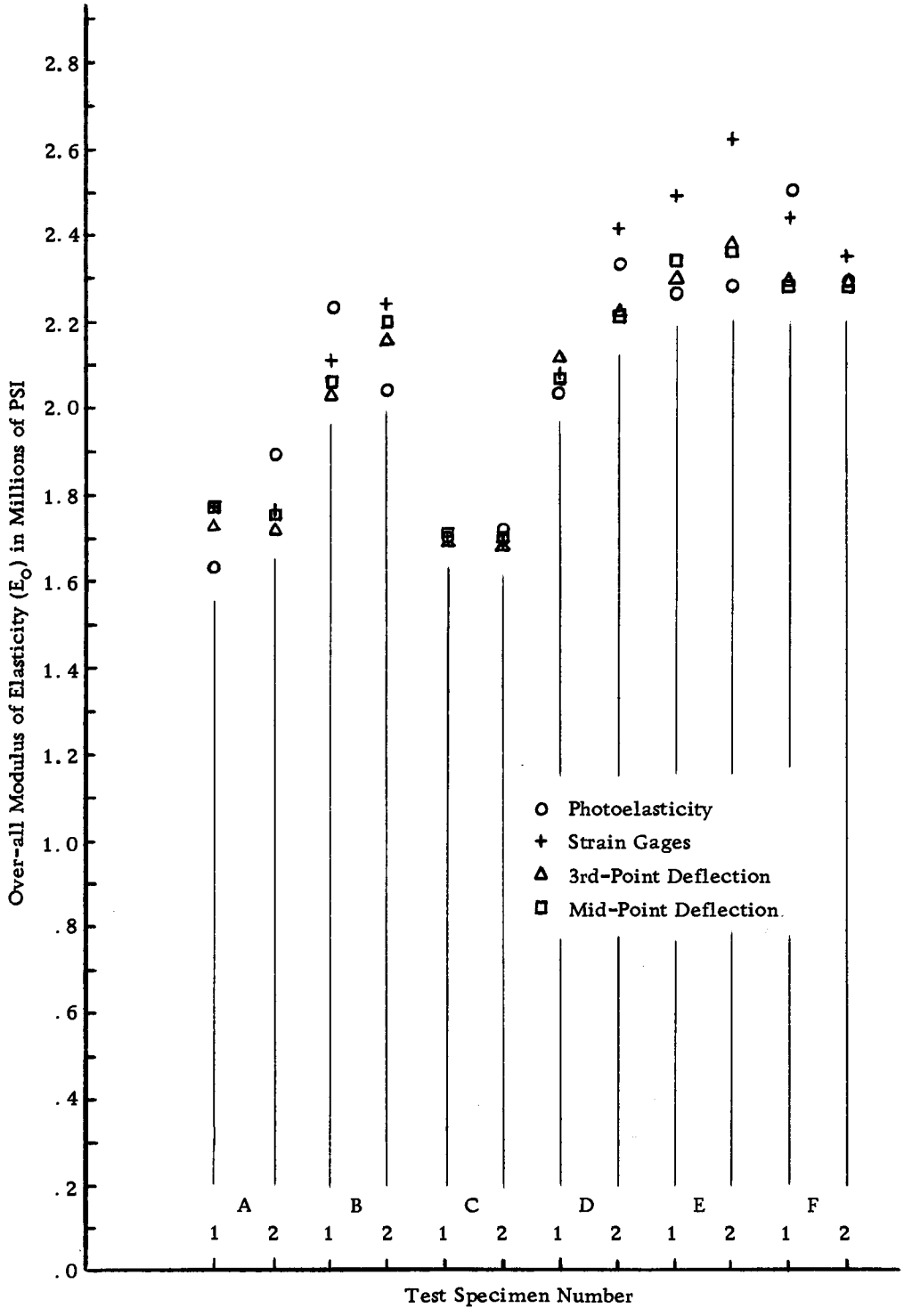

Figure 37. Comparison of test results.

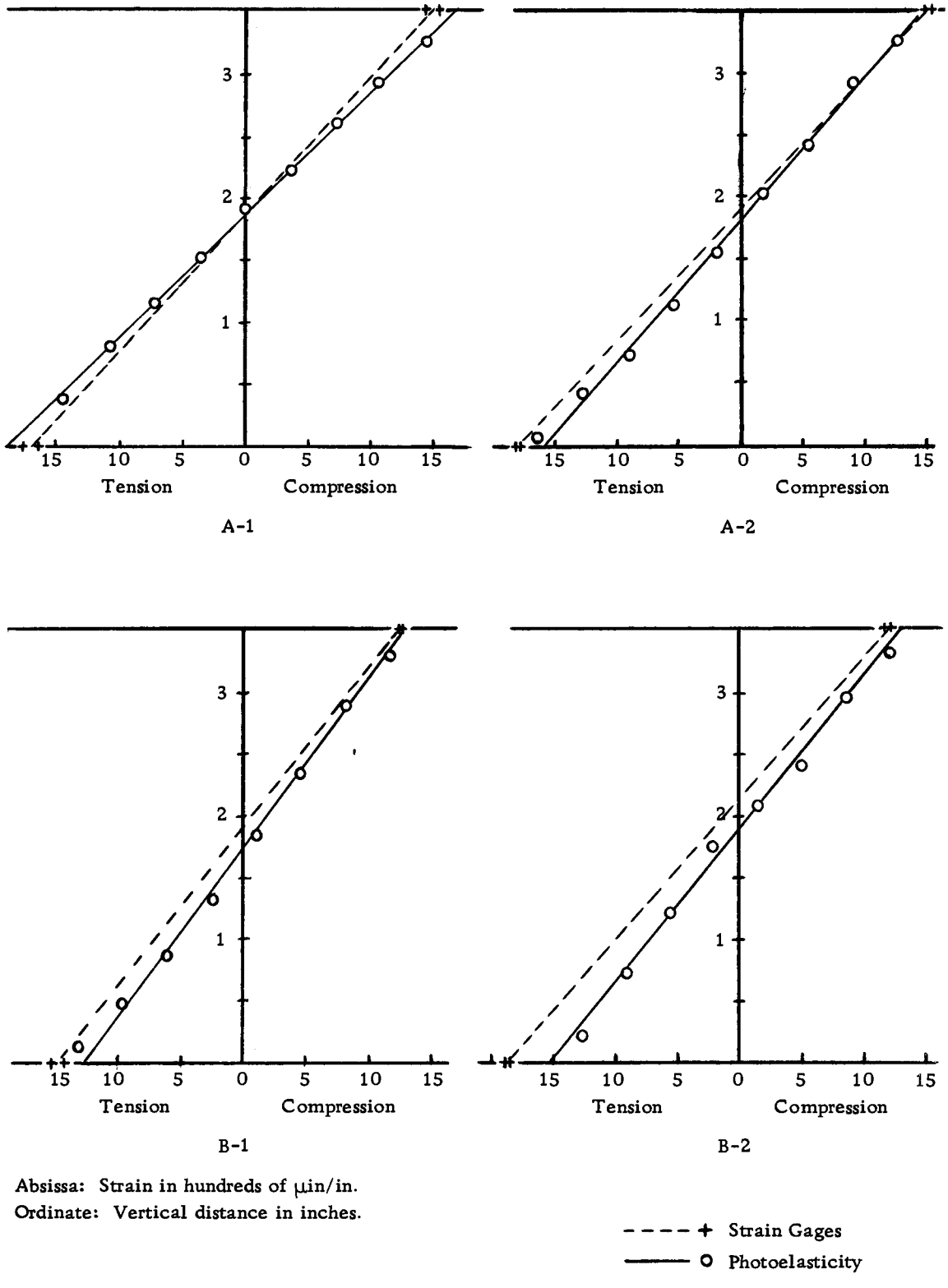

Figure 38. Strain distributions for specimens A-1, A-2, B-1, and B-2.

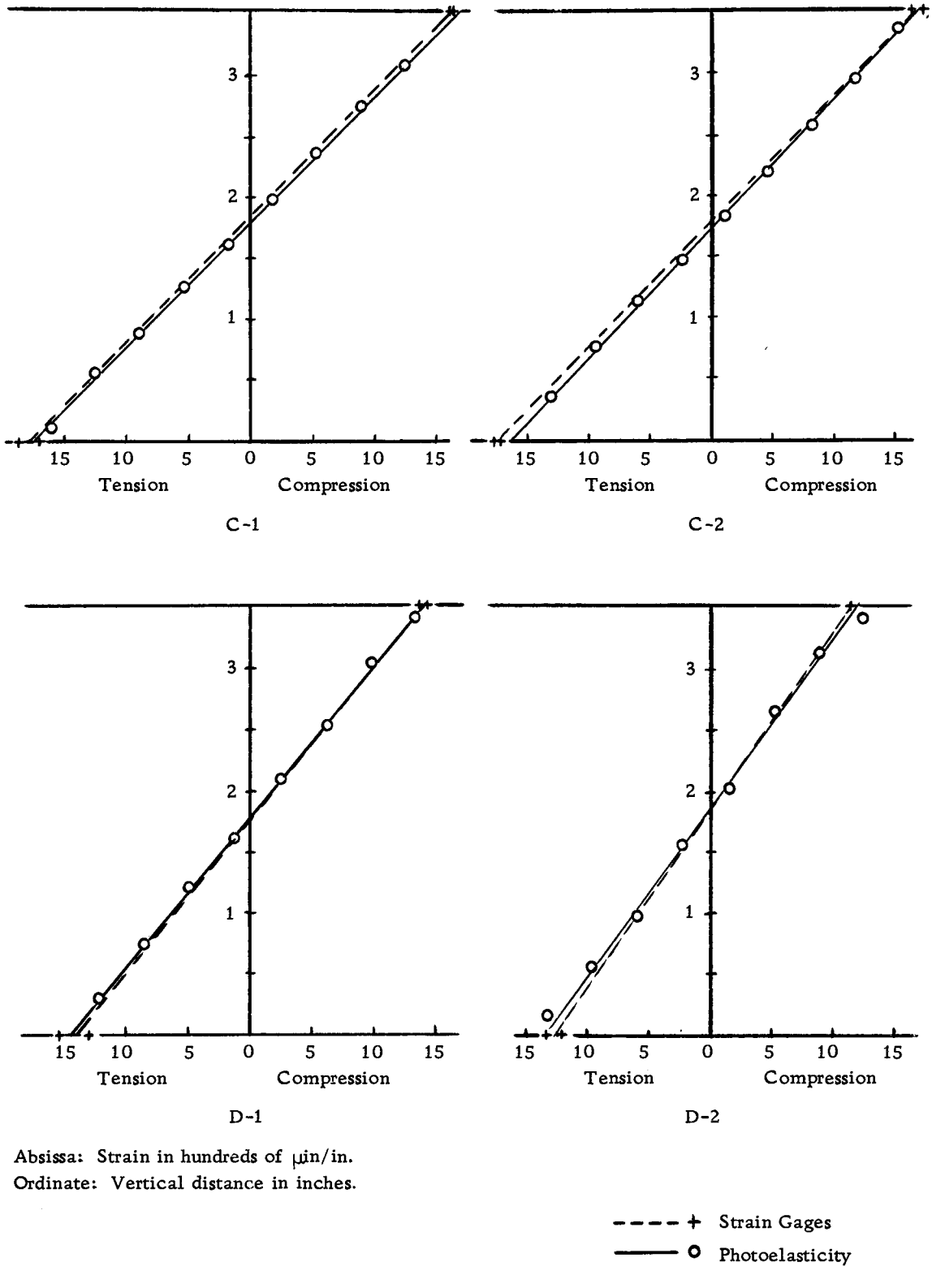

Figure 39. Strain distributions for specimens C-1, C-2, D-1, and D-2.

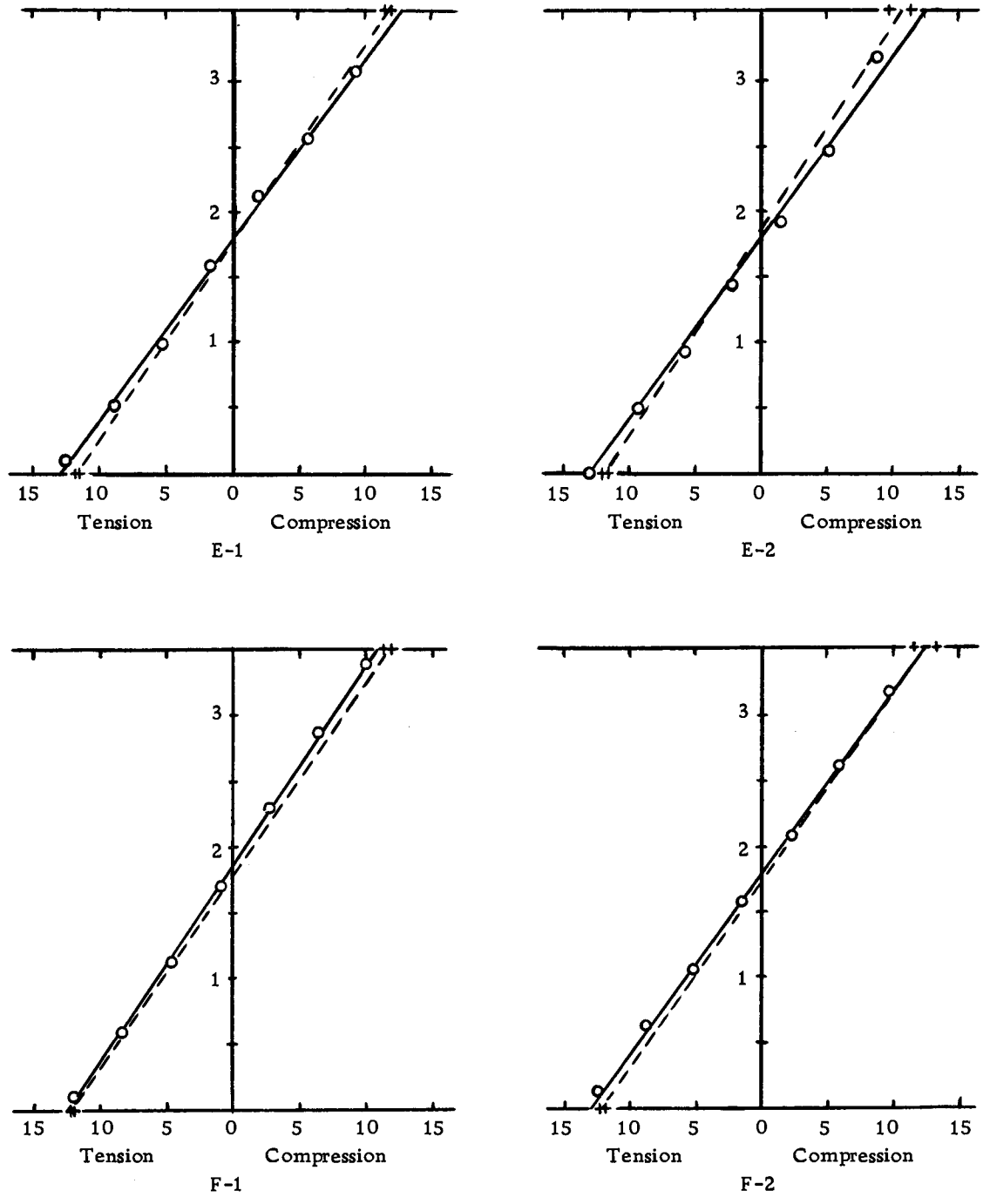

Absissa: Strain in hundreds of μin/in.
Ordinate: Vertical distance in inches.

---- + Strain Gages
——— o Photoelasticity

Figure 40. Strain distributions for specimens E-1, E-2, F-1, and F-2.

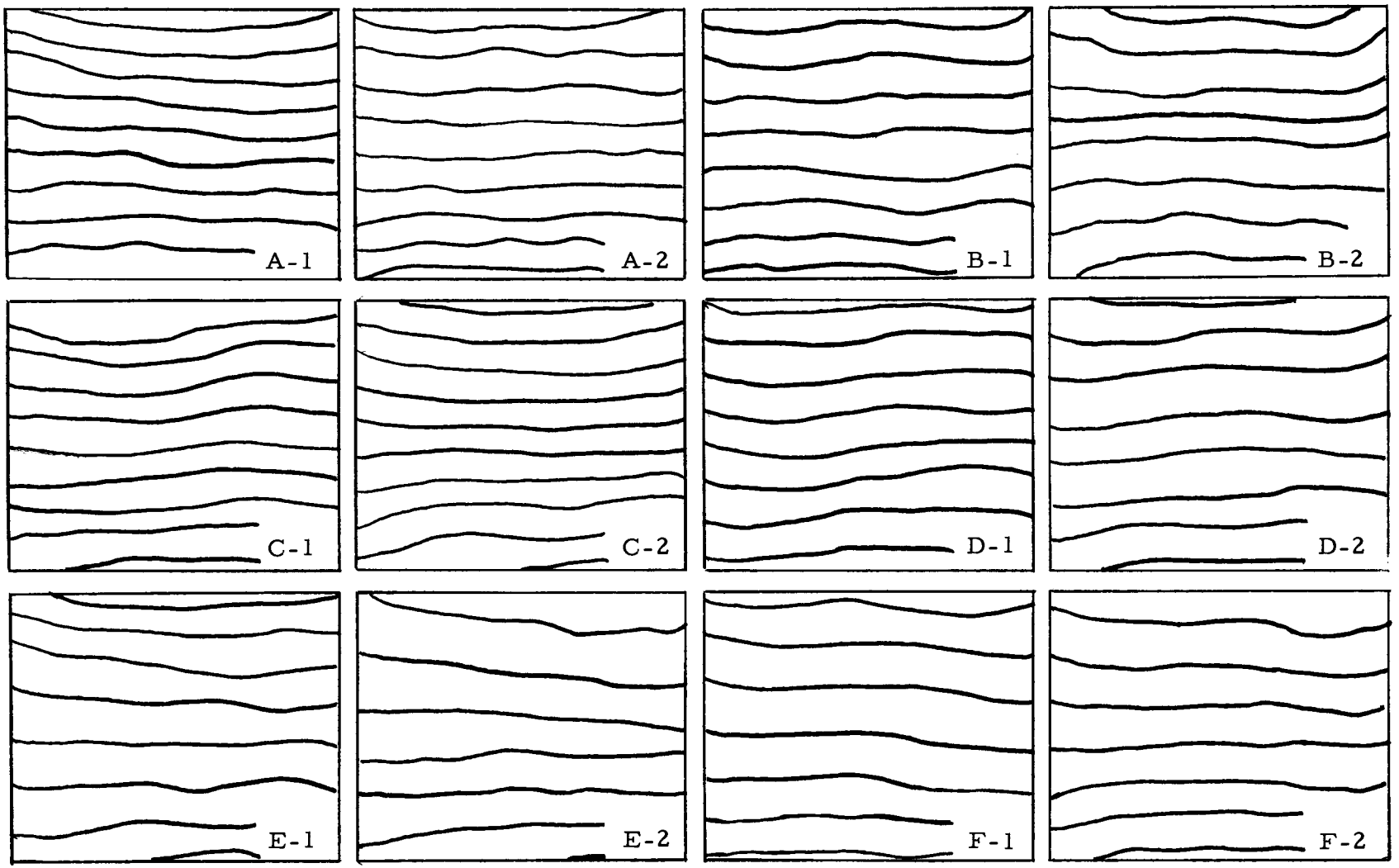

Figure 41. Photoelastic data tracings.

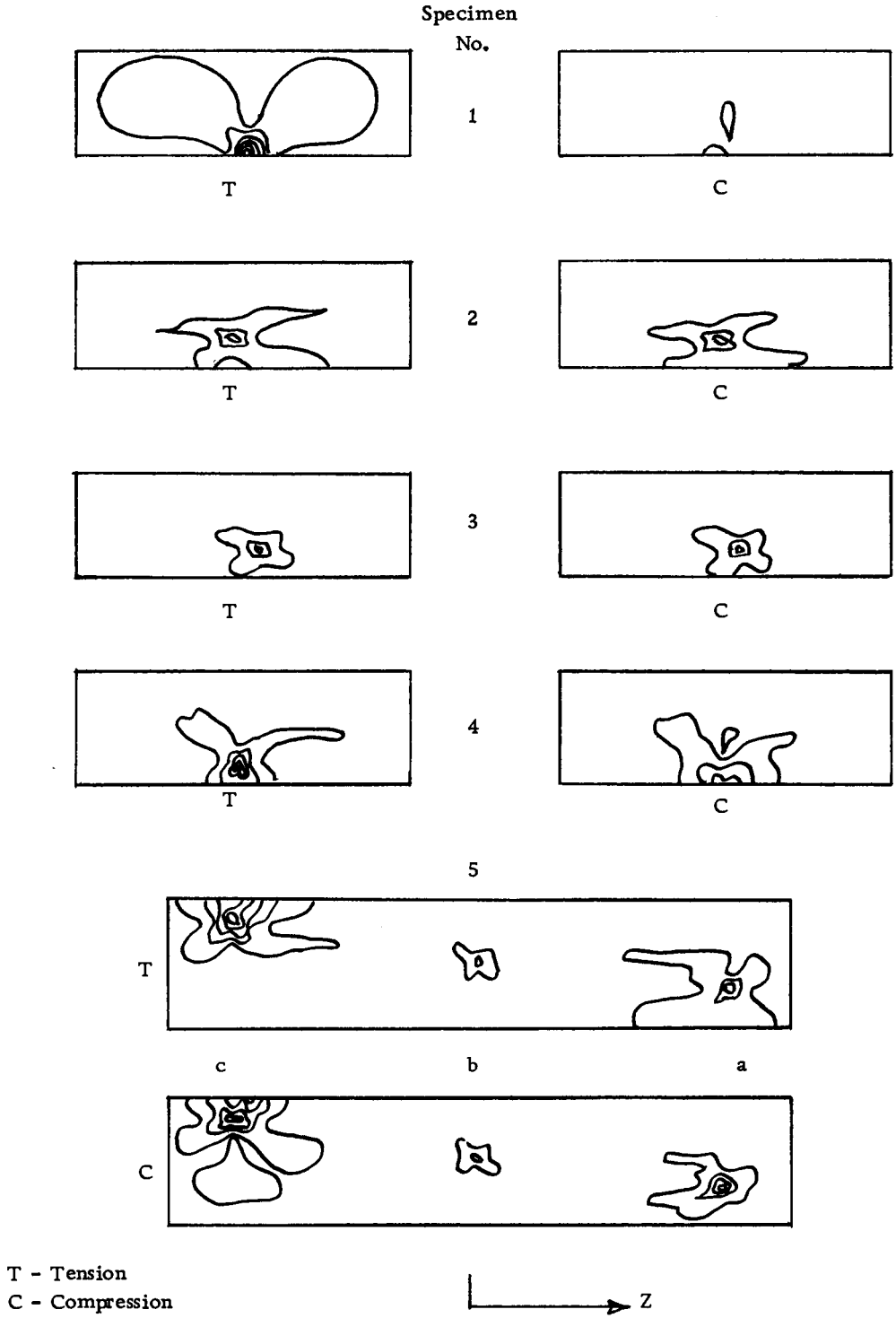

Figure 42. Laminated beam data tracings.

Table 1. List of various constants for comparative test specimens and computation of factors B and D from Eqs. (41) and (45).

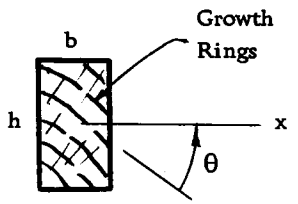

$M = 9750$ in-lb.

$I_x = \frac{bh^3}{12}$

$n = \sin\theta$

$m = \cos\theta$

$$B = \frac{1236}{I_x}\left[1 + \frac{h^2}{1268}(12.8n^2 + 15.6m^2)\right]$$

$$D = \frac{1053}{I_x}\left[1 + \frac{h^2}{1620}(12.8n^2 + 15.6m^2)\right]$$

Beam No.	b in.	h in.	h^2 in.^{2}	bh^3 in.^{3}	I_x in.^{4}	θ Degrees	Approximate n^2	Approximate m^2	B^{-1} in.	D^{-1} in.	$\frac{3M}{bh^2}$ psi
A-1	1.630	3.524	12.41	20.23	5.944	25	.153	.847	239.0	197.9	1445
A-2	1.633	3.525	12.42	20.30	5.960	25	.153	.847	238.1	197.3	1441
B-1	1.630	3.524	12.41	20.22	5.944	34	.345	.654	238.1	197.6	1447
B-2	1.634	3.530	12.47	20.35	5.989	34	.345	.654	236.0	196.0	1438
C-1	1.632	3.530	12.47	20.30	5.982	38	.345	.654	236.3	196.2	1442
C-2	1.634	3.532	12.48	20.40	6.000	37	.345	.654	235.8	195.7	1433
D-1	1.625	3.515	12.36	20.08	5.881	9	.024	.975	241.2	200.0	1457
D-2	1.628	3.520	12.39	20.17	5.942	9	.024	.975	239.0	197.9	1451
E-1	1.631	3.524	12.41	20.26	5.948	22	.153	.847	239.0	197.9	1444
E-2	1.627	3.521	12.40	20.16	5.918	21	.153	.847	240.0	198.8	1453
F-1	1.628	3.526	12.42	20.21	5.947	0	0.000	1.000	239.9	198.5	1447
F-2	1.630	3.524	12.41	20.25	5.944	0	0.000	1.000	240.0	198.8	1444

Table 2. Physical descriptions and maximum loads for laminated test beams.

$P = 77.4\ bh^2$

Beam No.	b in.	h in.	$bh^2/3$ in.	P lb.	Butt Joint Description
1	1.50	3.93	23.2	1800	1/64" Gap - well glued
2	1.50	3.25	15.8	1220	3/16" Gap - no glue
3	1.50	3.25	15.8	1220	3/32" Gap - no glue
4	1.60	3.45	19.0	1470	1/32" Gap - well glued
5	2.02	4.07	33.5	2590	(a) 1/16" Gap - no glue
					(b) no Gap - well glued
					(c) 1/32" Gap - no glue

Table 3. Deflection data for use in Eqs. (41) and (45).

Beam No.	Mid-Point Loading			Third-Point Loading		
	Trial I S	Trial II S	Average S	Trial I S	Trial II S	Average S
A-1	1362	1344	1353	1157	1127	1142
A-2	1362	1357	1360	1141	1150	1146
B-1	1160	1151	1156	975	968	972
B-2	1078	1065	1071	910	902	909
C-1	1395	1374	1384	1169	1157	1163
C-2	1387	1383	1385	1165	1170	1167
D-1	1160	1167	1163	947	946	946
D-2	1105	1056	1081	896	892	894
E-1	1023	1020	1021	856	860	858
E-2	1027	1007	1017	836	838	837
F-1	1056	1048	1052	867	868	868
F-2	1061	1047	1054	864	871	868

(All values in inches/lb.)

Table 4. Adjusted maximum fiber strains at P = 1500 lb. from strain gage data (all strains in μin/in).

Gage nos. 1 and 2 are compressive, 3 and 4 are tensile.

Beam No. and Gage No.		Individual Strains Trial I (1)	Individual Strains Trial II (2)	Average Ten. and Comp. Strains Trial I (3)	Average Ten. and Comp. Strains Trial II (4)	Average of (3) and (4) (5)
A-1	1	1550	1530	1510	1490	1500
	2	1470	1450			
	3	1660	1650	1725	1710	1720
	4	1790	1770			
A-2	1	1540	1530	1515	1505	1510
	2	1490	1480			
	3	1770	1790	1795	1795	1795
	4	1820	1800			
B-1	1	1260	1270	1280	1260	1270
	2	1300	1250			
	3	1450	1520	1505	1470	1490
	4	1560	1420			
B-2	1	1230	1220	1200	1195	1200
	2	1170	1170			
	3	1390	1390	1385	1380	1385
	4	1380	1370			
C-1	1	1610	1600	1620	1610	1615
	2	1630	1620			
	3	1700	1700	1785	1775	1780
	4	1870	1850			
C-2	1	1630	1650	1680	1695	1690
	2	1730	1740			
	3	1710	1710	1710	1710	1710
	4	1710	1710			
D-1	1	1340	1350	1380	1390	1385
	2	1420	1430			
	3	1290	1310	1410	1425	1420
	4	1530	1540			
D-2	1	1110	1150	1125	1140	1135
	2	1140	1130			
	3	1230	1230	1290	1290	1290
	4	1350	1350			
E-1	1	1140	1120	1165	1155	1160
	2	1190	1190			
	3	1160	1160	1170	1160	1165
	4	1180	1160			
E-2	1	970	970	1045	1055	1050
	2	1120	1140			
	3	1150	1160	1175	1185	1180
	4	1200	1210			
F-1	1	1200	1190	1170	1160	1165
	2	1140	1130			
	3	1210	1190	1215	1195	1205
	4	1220	1200			
F-2	1	1150	1170	1240	1260	1250
	2	1330	1350			
	3	1190	1270	1185	1235	1210
	4	1180	1200			

Table 5. Photoelastic data.

For the data in columns after (5): Top Figure--Vertical distance from bottom of beam to the fringe given at head of column (in inches).
Bottom Figure--Fringe given at head of column multiplied by figure in column (5)(in μin/in.).

Beam No.	Neutral axis (inches) (1)	ϵ_c μin/in. (2)	ϵ_t μin/in. (3)	ν_{zy} (4)	ϵ_z/n_f μ in/in. / fringe (5)	Compression Fringes				Tension Fringes					
						-2.0	-1.5	-1.0	-0.5	0	+0.5	+1.0	+1.5	+2.0	+2.5
A-1	1.81	1670	1890	.316	724	3.26	2.93	2.61	2.23	1.91	1.51	1.15	0.79	0.38	
						-1450	-1085	- 724	- 362	0	362	724	1085	1450	1810
A-2	1.84	1460	1600	.316	724		3.28	2.94	2.44	2.04	1.58	1.15	0.74	0.44	0.09
						-1450	-1085	- 724	- 362	0	362	724	1085	1450	1810
B-1	1.76	1300	1290	.346	708		3.31	2.90	2.36	1.85	1.33	0.89	0.49	0.14	
						-1420	-1060	- 708	- 354	0	354	708	1060	1420	1770
B-2	1.89	1310	1520	.346	708		3.35	2.96	2.42	2.09	1.76	1.22	0.73	0.22	
						-1420	-1060	- 708	- 354	0	354	708	1060	1420	1770
C-1	1.79	1680	1730	.346	708		3.08	2.75	2.38	1.98	1.61	1.26	0.88	0.56	0.12
						-1420	-1060	- 708	- 354	0	354	708	1060	1420	1770
C-2	1.75	1680	1650	.346	708	3.37	2.96	2.59	2.21	1.84	1.49	1.14	0.77	0.36	0.00
						-1420	-1060	- 708	- 354	0	354	708	1060	1420	1770
D-1	1.81	1420	1450	.297	734		3.42	3.03	2.52	2.10	1.61	1.21	0.75	0.31	
						-1470	-1100	- 734	- 367	0	367	734	1100	1470	1830
D-2	1.88	1180	1320	.297	734		3.42	3.13	2.64	2.01	1.54	0.95	0.53	0.13	
						-1470	-1100	- 734	- 367	0	367	734	1100	1470	1830
E-1	1.82	1260	1300	.316	724		3.52	3.06	2.55	2.12	1.57	0.98	0.50	0.10	
						-1450	-1085	- 724	- 362	0	362	724	1085	1450	1810
E-2	1.80	1250	1300	.316	724			3.18	2.47	1.92	1.44	0.92	0.49	0.00	
						-1450	-1085	- 724	- 360	0	362	724	1085	1450	1810
F-1	1.87	1090	1230	.292	737			3.41	2.89	2.31	1.72	1.13	0.59	0.11	
						-1470	-1100	- 737	- 368	0	368	737	1100	1470	1840
F-2	1.81	1220	1300	.292	737			3.18	2.61	2.09	1.59	1.05	0.63	0.13	
						-1470	-1100	- 737	- 368	0	368	737	1100	1470	1840

Table 6. Final results of all comparative tests.

Beam No.	Deflection Mid-Point E_o (1)	Deflection Third-Point E_o (2)	Strain Gages E_o (3)	Photoelasticity E_o (4)
A-1	1.77	1.73	1.77	1.63
A-2	1.75	1.72	1.76	1.89
B-1	2.06	2.03	2.11	2.23
B-2	2.20	2.16	2.24	2.04
C-1	1.71	1.69	1.70	1.70
C-2	1.70	1.68	1.69	1.72
D-1	2.07	2.12	2.08	2.03
D-2	2.21	2.22	2.41	2.33
E-1	2.34	2.30	2.49	2.26
E-2	2.36	2.38	2.62	2.28
F-1	2.28	2.29	2.44	2.50
F-2	2.28	2.29	2.35	2.29

(All values in millions of psi.)

Table 7. Regression relations between test variables.

Function	Intercept a 10^6 psi	Slope b	Std. Deviation σ 10^6 psi	Confidence Interval I 90% Absolute 10^6 psi	90% % of Mean	95% Absolute 10^6 psi	95% % of Mean
$M = a + bP \pm I$	.361	.819	.118	.214	10.4	.263	12.8
$T = a + bP \pm I$	.263	.862	.121	.220	10.7	.270	13.2
$M = a + bS \pm I$	.439	.758	.045	.082	4.0	.100	4.9
$T = a + bS \pm I$	.359	.791	.052	.094	4.6	.116	5.7
$M = a + bT \pm I$	.112	.950	.027	.049	2.4	.060	2.9

M - Mid-point loading deflection test data (E in psi)

T - Third-point loading deflection test data (E in psi)

P - Photoelastic coating test data (E in psi)

S - Strain gage test data (E in psi)

APPENDIX B

MISCELLANEOUS CALCULATIONS AND INFORMATION

MISCELLANEOUS CALCULATIONS AND INFORMATION

Laminated Beam Test Load Computation

Find: Load P required to put a stress of 3020 psi in extreme fibers of pure bending zone.

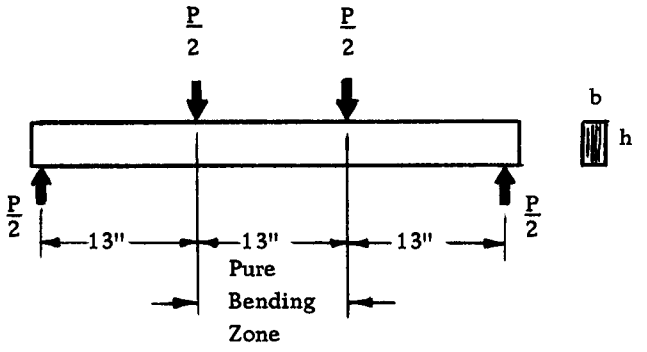

Figure 42. Typical laminated test beam.

The center section is seen to sustain a pure bending moment (no shear) of

$$M = (13)(P/2).$$

From beam theory

$$\sigma = \frac{Mc}{I} \qquad \text{or} \qquad M = \frac{bh^3\sigma}{12c}$$

where c is the distance from the neutral axis and is equal to h/2 for extreme fibers. Thus,

$$(13)(P/2) = \frac{bh^2\sigma}{6}.$$

And since σ must be 3020 psi

$$P = (3020/39)\,bh^2 = 77.4\,bh^2 .$$

P is computed for each specimen in Table 2 (p. 120).

Photoelastic Coating Material Used in Tests

Manufacturer:	Photolastic, Inc. 176 Lincoln Highway Malvern, Pennsylvania
Material Code:	PS-1B
Strain-Optic Coefficient:	K = 0.14
Strain Sensitivity:	f = 940 μin/in/fringe
Thickness:	t = 0.084 $\pm$ .001 in.
Adhesive Code:	PC-1